

HyperJump: Accelerating HyperBand via Risk Modelling

Pedro Mendes^{1,2}, Maria Casimiro^{1,2}, Paolo Romano¹

¹INESC-ID and Instituto Superior Técnico, Universidade de Lisboa

²Institute for Software Research, Carnegie Mellon University

{pgmendes, mdaloura}@andrew.cmu.edu, romano@inesc-id.pt

Abstract

In the literature on hyper-parameter tuning, a number of recent solutions rely on low-fidelity observations (e.g., training with sub-sampled datasets or for short periods of time) to extrapolate good configurations to use when performing full training. Among these, HyperBand is arguably one of the most popular solutions, due to its efficiency and theoretically provable robustness.

In this work, we introduce HyperJump, a new approach that builds on HyperBand’s robust search strategy and complements it with novel model-based risk analysis techniques that accelerate the search by *jumping* the evaluation of low risk configurations, i.e., configurations that are likely to be discarded by HyperBand. We evaluate HyperJump on a suite of hyper-parameter optimization problems and show that it provides over one-order of magnitude speed-ups, both in sequential and parallel deployments, on a variety of deep-learning and kernel-based learning problems when compared to HyperBand as well as to a number of state of the art optimizers.

1 Introduction

Hyper-parameter tuning is a crucial phase to optimize the performance of machine learning (ML) models, which is notoriously expensive given that it typically implies repeatedly training models over large data sets. State-of-the-art solutions address this issue by exploiting cheap, low-fidelity models (e.g., trained with a fraction of the available data) to extrapolate the quality of fully trained models.

HyperBand (Li et al. 2018), henceforth referred to as HB, is probably one of the most popular solutions in this area. HB is based upon a randomized search procedure, called Successive Halving (SH) (Jamieson and Talwalkar 2016), which operates in stages of fixed “budget” (e.g., training time or training set size): at the end of stage i , the best performing $1/\eta\%$ configurations are selected to be evaluated in stage $i + 1$, where they will be allocated $\eta \times$ larger budget. By restarting the SH procedure over multiple, so called, brackets using different initial training budgets, HB provides theoretical guarantees of convergence to the optimum, incurring negligible computational overheads and outperforming state-of-the-art optimizers (e.g., based on Bayesian Optimization (BO) (Brochu, Cora, and de Freitas 2010)) that do

Copyright © 2022, Association for the Advancement of Artificial Intelligence (www.aaai.org). All rights reserved.

not exploit low-fidelity observations. However, the random nature of HB also inherently limits its efficiency, as shown by recent model-based multi-fidelity approaches (Falkner, Klein, and Hutter 2018; Klein et al. 2017).

This work introduces HyperJump (HJ), a novel hyper-parameter optimization method that builds upon HB’s robust search strategy and accelerates it via an innovative, model-based technique. In a nutshell, the idea at the basis of HJ is to “jump” (i.e., skip either partially or entirely) some of HB’s stages. To minimize the risks associated with jumps, while maximizing the attainable gains by favoring earlier jumps, HJ exploits, in a synergistic way, three new mechanisms:

- A novel modelling technique to predict the risk of jumping, which we call Expected Accuracy Reduction (EAR). The EAR exploits the model’s uncertainty in predicting the quality of untested configurations as a basis to estimate the expected reduction in the accuracy between (i) the best configuration included in the stage reached after a jump and (ii) the best configuration discarded due to the jump.
- A criterion for selecting the configurations to include in the HB stage targeted by a jump, which aims to minimize the jump’s risk. This is a combinatorial problem¹, which we tackle via a lightweight heuristic that has logarithmic complexity with respect to the number of configurations in the target stage of the jump.
- A method for prioritizing the testing of configurations in a stage that aims to increase the likelihood of jumping, by favouring the sampling of configurations that are expected to yield the highest risk reduction for future jumps.

We compare HJ with a number of state-of-the-art optimizers (Li et al. 2018; Klein et al. 2017; Snoek, Larochelle, and P. Adams 2012; Falkner, Klein, and Hutter 2018; Li et al. 2020) on a suite of hyper-parameter optimization problems, on both sequential and parallel deployments, and show that HJ can provide over one-order of magnitude speed-ups on a variety of deep-learning and kernel-based learning problems. We also conduct an ablation study that sheds light on the contributions of the various mechanisms employed by HJ on its performance.

¹The number of candidate configuration sets for a jump to a stage with k configurations from one with n configurations is $\binom{n}{k}$.

2 Related Work

Existing hyper-parameter techniques can be coarsely classified along two dimensions: **i**) whether they use model-free or model-based approaches; **ii**) whether they exploit solely high-fidelity evaluations or also multi-fidelity ones.

As already mentioned, HB is arguably one of the most prominent model-free approaches. Its random nature, combined with its SH-based search algorithm, makes it not only provably robust, but also efficiently parallelizable (Li et al. 2018; Falkner, Klein, and Hutter 2018; Li et al. 2020) and, overall, very competitive and lightweight.

As for the model-based approaches, recent literature on hyper-parameter optimization has been dominated by Bayesian Optimization (BO) (Brochu, Cora, and de Freitas 2010) methods. BO relies on modelling techniques (e.g., Gaussian Processes (Rasmussen and Williams 2006), Random Forests (Breiman 2001) or Tree Parzen Estimator (TPE) (Bergstra et al. 2011)) to build a surrogate model of the function $f : \mathcal{X} \rightarrow \mathcal{R}$ to be optimized. The surrogate model is then used to guide the selection of the configurations to test via an *acquisition function* that tackles the exploration-exploitation dilemma. A common acquisition function is the Expected Improvement (EI) (Mockus, Tiesis, and Zilinskas 1978), which exploits information of the model’s uncertainty on an untested configuration c to estimate by how much c is expected to improve over the current incumbent.

Swersky et al. (Swersky, Snoek, and Adams 2013) were probably the first to propose an adaptation of the BO framework to take advantage of low-fidelity evaluations obtained using a training set of smaller dimensions. This idea was extended in Fabolas (Klein et al. 2017), which learns the lowest-fidelities that provide more knowledge about the optimum. A related body of work (Swersky, Snoek, and Adams 2014; Domhan, Springenberg, and Hutter 2015; Dai et al. 2019; Golovin et al. 2017) uses models (typically GPs) to predict the loss of a neural network as a function of both the hyper-parameters and the training iterations. Models are then used to extrapolate the full-training loss and cancel under-performing training runs.

From a methodological perspective, the fundamental difference between HJ and this body of model-based works lies in the type of problems that are addressed by their modelling techniques. Since HJ builds on HB’s search strategy, it uses models to answer a relatively simple question: quantify the risk of discarding high quality configurations by accelerating one or more HB stages. The above mentioned works, conversely, being solely model based, need to employ sophisticated modelling techniques to answer complex questions, such as selecting the cheapest configuration to test in order to maximize the information gain on the optimum (Klein et al. 2017; Swersky, Snoek, and Adams 2013) or what is the earliest epoch in which a given train run can be deemed sub-optimal and terminated. By using models to address such complex questions, these techniques require computationally expensive implementations, which can impose significant overhead especially when the cost of evaluating configurations is relatively cheap (e.g., when using low-fidelity observations) (Sec. 4). By taking advantage of the (theoret-

Algorithm 1: Pseudo-code for a HJ bracket consisting of S stages, with budget b for the initial stage.

```

1: Set(Config)  $C = \text{GET\_CONFIGS\_FOR\_BRACKET}()$             $\triangleright$  Model-driven bracket
   warmstart (§ 3.4)
2: Set(Config)  $T = \emptyset$ ; Set(Config)  $U = C$ ;            $\triangleright$   $T$  and  $U$  contain the tested/untested
   configs, resp.
3: for  $s \in \{0, \dots, S - 1\}$  do                                 $\triangleright$   $s$  denotes the current stage
4:   bool jump = false;
5:   while  $U \neq \emptyset$  do            $\triangleright$  Test configs. in curr. stage, or jump to a future stage
6:      $\langle \text{target}, \mathcal{S} \rangle = \text{EVALUATE\_JUMP\_RISK}(s, T, U)$             $\triangleright$  HJ risk-analysis
   (Sec. 3.2)
7:     if target  $\neq s$  then            $\triangleright$  Jump to target stage
8:        $s = \text{target}$ ;  $T = U = \emptyset$ ;  $C = \mathcal{S}$ ; jump = true; break;
9:     else
10:       $c = \text{NEXT\_CONF\_TO\_TEST}(U, b\eta^s)$ ;            $\triangleright$  Next selected
        config. minimizes future risk (Sec. 3.3)
11:      acc = evaluate_config( $c, b\eta^s$ )            $\triangleright$  Measure config.  $c$  with budget  $b\eta^s$ 
        and return its accuracy
12:       $T = T \cup \{c\}$ ;  $U = U \setminus \{c\}$ 
13:      update_model( $\langle c, b\eta^s, acc \rangle$ )
14:    end if
15:  end while
16:  if  $\neg$ jump then            $\triangleright$  Use HB’s policy if HJ did not trigger a jump by the end of
   the stage
17:     $U = C = \text{topK}(C, |C|\eta^{-1})$             $\triangleright$  test top  $1/|\eta|$ % configs. in next stage
18:  end if
19: end for

```

ically provable) robustness of HB, which HJ accelerates in a risk-aware fashion via model-driven techniques, we argue that HJ fuses the best of both worlds: it preserves HB’s theoretical robustness (Sec. 3.6), while accelerating it by more than one order of magnitude via the use of lightweight, yet effective, models (as we will show experimentally).

The works more closely related to HJ are a number of recent approaches, e.g., (Falkner, Klein, and Hutter 2018; Wang, Xu, and Wang 2018; Bertrand et al. 2017) that extend HB with BO to warm start it, i.e., to select (a fraction of) the configurations to include in a new HB bracket. This mechanism, which HJ also incorporates (Sec. 3.4), is complementary to the key novel idea exploited by HJ to accelerate HB, i.e., short-cutting the SH process by skipping to later SH stages in low risk scenarios. As we will show via an ablation study comparing the impact of the various mechanisms employed by HJ, “jumping” is clearly the one that contributes the most to HJ’s efficiency. Further, when compared with BOHB (Falkner, Klein, and Hutter 2018), which warm starts HB using BO, HJ provides more than one order of magnitude speed-ups.

3 HyperJump

As already mentioned, a HB bracket is composed of up to S_{\max} stages, where $S_{\max} = \lfloor \log_\eta(R) \rfloor$. R is the maximum “budget” allocated to the evaluation of a hyper-parameter configuration and η is an exponential factor (typically 2 or 3) that controls the increase/decrease of the allocated budget/number of tested configurations in two consecutive stages of the same bracket.

The pseudo-code in Alg. 1 overviews the various mech-

anisms employed by HJ to accelerate a single HB bracket composed of $S < S_{max}$ stages. The bracket’s initial stage allocates a budget b , where $b = R\eta^{-(S-1)}$, as prescribed by HB. HJ leverages two main mechanisms to accelerate the execution of a HB bracket, which are encapsulated in the functions EVALUATE_JUMP_RISK and GET_NEXT_CONFIG_TO_TEST.

EVALUATE_JUMP_RISK is executed within HJ’s inner loop (Alg. 1, line 6), to decide whether to stop testing configurations in the current stage and jump to a later stage. This function takes as input the current stage, s , and the configurations already and still to be tested, T and U . It returns the pair $\langle target, \mathcal{S} \rangle$ where $target$ denotes the stage to jump to (in which case $target \neq s$) and \mathcal{S} the selected configurations for the target stage. We detail this function in Sec. 3.2.

If the risk of jumping is deemed too high, HJ continues testing the configurations in the current stage. Unlike HB, which uses a random order of exploration, HJ prioritizes the order of exploration via the NEXT_CONF_TO_TEST function (Alg. 1, line 10). This function seeks to identify a configuration whose evaluation will lead to a large reduction of the risk of jumping, so as to favour early jumps and enhance the efficiency of HJ. We discuss how we implement this function in Sec. 3.3. After testing configuration c in budget $b\eta^s$ and measuring its accuracy acc , we update the models used to predict the accuracy of untested configurations (with different budgets). We discuss the type of models used by HJ in Sec. 3.1. Finally, GET_CONFIGS_FOR_BRACKET (Alg. 1, line 1) encapsulates the model’s logic to select the configurations to be included in a new bracket, which we detail in Sec. 3.4.

3.1 Modelling configurations’ quality

HJ’s risk analysis methodology relies on GP-based models to estimate the accuracy of a configuration c in a given budget. As in recent related works, e.g., (Klein et al. 2017, 2020; Mendes et al. 2020), we include in the feature space of the GP models not only the hyper-parameters’ space, but also the budget (so as to enable inter-budget extrapolation). Further, analogously to, e.g., (Klein et al. 2017; Mendes et al. 2020), we employ a custom kernel that encodes the expectation that the loss function has an exponential decay with larger budgets along with a generic Matérn 5/2 kernel that is used to capture relations among the hyper-parameters.

3.2 Deciding whether to jump

We address the problem of deciding whether to adopt HB’s default policy or skip some, or even all of, the future stages of the current bracket by decomposing it into three simpler sub-problems: **1)** modelling the risk of jumping from the current stage to the next stage while retaining an arbitrary subset \mathcal{S} of the configurations C in the current stage; **2)** identifying “good” candidates for the subset of configurations to retain after a jump from stage s to stage $s+1$, i.e., configurations that, if included in the target stage of the jump, reduce the risk of jumping; **3)** generalizing the risk modelling to jumps that skip an arbitrary number of stages.

Next, we discuss how we address each sub-problem.

1) Modelling the risk of jumping to the next stage. Let us start by discussing how we model the risk of jumping from a source (current) stage s to a target stage t that is the immediate successor of s ($t=s+1$). Consider C the configurations in s ; T and U the tested/untested configurations in s , resp., and \mathcal{S} and \mathcal{D} the subset of configurations in C that are selected/discard, resp., when jumping to stage t .

Our modelling approach is based on the observation that short-cutting HB’s search process and jumping to the next stage exposes the risk of discarding the configuration that achieves maximum accuracy in the current stage (and that may turn out to improve the current incumbent, when tested in full-budget). This risk can be modelled as the difference between two random variables:

$$\mathcal{A}_s^{\mathcal{D}} = \max_{c_i \in \mathcal{D}} A(c_i, b\eta^s), \quad \mathcal{A}_s^{\mathcal{S}} = \max_{c_k \in \mathcal{S}} A(c_k, b\eta^s)$$

defined as the maximum accuracy of the configurations in the set of discarded and selected configurations in stage s , respectively. From a mathematical standpoint, we only require \mathcal{A} to be finite, so that the maximum and difference operators are defined. So one may use arbitrary accuracy metrics provided that they match this assumption, e.g., even unbounded, but finite, metrics like negative log likelihood.

One can then quantify the “absolute” risk of a jump from stage s to stage $s+1$, which we call Expected Accuracy Reduction (EAR) (Eq. 1), as the expected value of the difference between these two variables, restricted to the scenarios in which configurations with higher accuracy are discarded due to jumping (i.e., $\mathcal{A}^{\mathcal{D}} - \mathcal{A}^{\mathcal{S}} > 0$):

$$\begin{aligned} EAR_s^{s+1}(\mathcal{D}, \mathcal{S}) &= \int_{-\infty}^{+\infty} P(\mathcal{A}_s^{\mathcal{D}} - \mathcal{A}_s^{\mathcal{S}} = x) \max\{\mathcal{A}_s^{\mathcal{D}} - \mathcal{A}_s^{\mathcal{S}}, 0\} dx \\ &= \int_0^{+\infty} x P(\mathcal{A}_s^{\mathcal{D}} - \mathcal{A}_s^{\mathcal{S}} = x) dx \end{aligned} \quad (1)$$

The EAR is computed as follows. The configurations in \mathcal{D} and \mathcal{S} are either untested or already tested. In the former case, we model their accuracy via a Gaussian distribution (given by the GP predictors); in the latter case, we model their accuracy either as a Dirac function (assuming noise-free measurements, which is HJ’s default policy) or via a Gaussian distribution (whose variance can be used to model noisy measurements). In any case, the PDF and CDF of $\mathcal{A}^{\mathcal{D}}$ and $\mathcal{A}^{\mathcal{S}}$ can be computed in closed form. Instead, computing the difference between these two random variables requires solving a convolution that cannot be determined analytically. Fortunately, both this convolution and the outer integral in Eq. 1 can be computed in a few mssecs using open source numerical libraries (Sec. 4). Additional details on the computation of the EAR are provided in the supplemental material.

Next, we introduce the rEAR (relative EAR), which is obtained by normalizing the EAR by the loss of the current incumbent, noted l^* : $rEAR_s^{s+1}(\mathcal{D}, \mathcal{S}) = EAR_s^{s+1}(\mathcal{D}, \mathcal{S})/l^*$. The rEAR estimates the “relative” risk of a jump and can be interpreted as the percentage of the maximum potential for improvement that is expected to be sacrificed by a jump. In HJ, we consider a jump “safe” if its corresponding rEAR is

below a threshold λ , whose default value we set to 10%. As we show in the supplemental material, in practical settings, HJ has robust performances for a large range of (reasonable) values of λ . One advantage of using the rEAR, instead of the EAR as risk metric is that the rEAR allows for naturally adapting the risk propensity of HJ’s logic, making HJ progressively less risk prone as the optimization process evolves and better incumbents are found.

2) Identifying the safest set of configurations for a jump. Determining the safest subset of configurations to include when jumping to the next stage via naive, enumerative methods would have prohibitive costs, as it would require evaluating the rEAR for all possible subsets \mathcal{S} of size $|C|/\eta$ of the configurations in the current stage s . For instance, assuming $\eta=3$, $|C|=81$ and that less than half of the configurations in C were tested, the number of distinct target sets for a jump of a single stage is $\binom{81}{27} \approx 2E21$.

We tackle this problem by introducing an efficient, model-driven heuristic that recommends a total of $1+2\lfloor\log_\eta|\mathcal{S}|\rfloor$ candidates for \mathcal{S} . The first candidate set evaluated by HJ, denoted \mathcal{K} is obtained by considering the top $|\mathcal{S}|$ configurations, ranked based on their actual or predicted accuracy depending on whether they have already been tested or not.

Next, using \mathcal{K} as a template, we generate $\lfloor\log_\eta|\mathcal{S}|\rfloor$ alternative sets by replacing the worst $|\mathcal{S}|/\eta^i$ ($1 \leq i \leq \lfloor\log_\eta|\mathcal{S}|\rfloor$) configurations in \mathcal{K} with the next best configurations in $C \setminus \mathcal{K}$, ranked based on their (predicted/measured) accuracy.

We further generate $\lfloor\log_\eta|\mathcal{S}|\rfloor$ alternative candidate sets by exploiting model uncertainty as follows: we identify the worst $|\mathcal{S}|/\eta^i$ configurations in \mathcal{K} , ranked according to their lower confidence bound, and replace them with the configurations in $C \setminus \mathcal{K}$ that have the highest confidence (we use a confidence bound of 90%). Intuitively, this way we remove from the reference set \mathcal{K} the configurations that are likely to have lower accuracy if the model overestimated their mean. These are replaced by the configurations that, although having lower (average) predicted accuracy, have the potential to achieve high accuracy, given the model’s uncertainty.

The pseudo-code of this heuristic and diagrams illustrating its behavior can be found in the supplemental material.

3) Generalizing to multi-hop jumps. Alg. 2 shows how to compute the rEAR of a jump that skips $j > 1$ stages from the current stage s . This is done in an iterative fashion by computing the rEAR for jumps from stage $s + i$ to stage $s + i + 1$ ($i \in [1, j - 1]$) and accumulating the corresponding rEARs to yield the rEAR of the jump.

At each iteration, the candidate sets for the set \mathcal{S} of configurations to be retained after the jump are obtained via the GET_CANDIDATES_FOR_ \mathcal{S} function (which encapsulates the logic just described in point 2). Among these $1+2\lfloor\log_\eta|\mathcal{S}|\rfloor$ candidate sets, the one with minimum risk is identified. The process is repeated replacing C with the candidate set that minimizes the risk of the current jump (line 11), until λ is exceeded, thus seeking to maximize the “jump length”, i.e., the number of stages that can be safely skipped. As such, the computation of the risk of a jump from a stage with $|C|$ configurations and that skips $j > 1$ stages requires $\mathcal{O}(j(1 + \log_\eta|C|/\eta))$ rEAR evaluations. This ensures the

Algorithm 2: Pseudo-code for the EVALUATE_JUMP_RISK function.

```

1: <int s, Set<Config>  $\mathcal{S}\mathcal{S} = \emptyset$ ;  $C = \text{Tested} \cup \text{Untested}$ .
3: while  $s < S$  do  $\triangleright \mathcal{S}$ : maximum number of stages
4:   Set<Set<Config>> candidates = GET_CANDIDATES_FOR_ $\mathcal{S}$ (Tested, Untested, s)
5:   minRisk = min $_{\mathcal{X} \in \text{candidates}}$  rEAR $^{s+1}_s(\mathcal{X}, C \setminus \mathcal{X})$ 
6:    $\mathcal{S} = \arg\min_{\mathcal{X} \in \text{candidates}} \text{rEAR}^{s+1}_s(\mathcal{X}, C \setminus \mathcal{X})$   $\triangleright \mathcal{S}$ : Set that minimizes the risk
7:   if rEAR + minRisk >  $\lambda$  then
8:     return  $\langle s, \mathcal{S} \rangle$   $\triangleright$  Return the target stage and the set with selected configs.
9:   else  $\triangleright$  Try to extend the jump by one hop
10:    rEAR += minRisk; s++
11:     $C = \text{Untested} = \mathcal{S}$ ; Tested =  $\emptyset$ 
12:   end if
13: end while
14: return  $\langle s, \emptyset \rangle$   $\triangleright$  Jump all stages in the current bracket and start a new bracket

```

scalability of HJ’s risk analysis methodology even when considering jumps that can skip a large number of stages.

3.3 Reducing the risk to jump by prioritizing the evaluation order of configurations

HJ also uses a model-based approach to determine in which order to evaluate the configurations of a stage. This mechanism aims to enhance HJ’s efficiency by prioritizing the evaluations of configurations that are expected to yield the largest reduction of risk for future jumps.

The literature on look-ahead non-myopic BO (Yue and Kontar 2020; Casimiro et al. 2020; Lam, Willcox, and Wolpert 2016; Lam and Willcox 2017) has already investigated several techniques aimed at predicting the impact of future exploration steps on model-driven optimizers. These approaches often impose large computational overheads, due to the need of performing expensive “simulations”, i.e., re-training the models to simulate alternative evaluation outcomes, and to their ambition to maximize long-term rewards (in contrast to the greedy nature of typical BO approaches).

Motivated by our design goal of keeping HJ lightweight and scalable, we depart from these modelling approaches and employ a simpler, greedy heuristic that allows for estimating the impact of evaluating an untested configuration without requiring expensive model retrains. More in detail, we simulate the evaluation of an untested configuration c by querying the model (without retraining it) and including c in the set of tested configurations (using the model predicted accuracy for c as its ground truth). Next, we execute the EVALUATE_JUMP_RISK function to obtain the updated risk of jumping and the corresponding target stage. We repeat this procedure for all the untested configurations in the stage, and select, as the next to test, the one that enables the longest safest jump (determined via the EVALUATE_JUMP_RISK function). The pseudo-code of this mechanism can be found in the supplemental material.

3.4 Selecting the configurations for a new bracket

To further accelerate HB, HJ leverages BO to determine which configurations to include when a new bracket is started — an idea already exploited in prior work, e.g., (Falkner, Klein, and Hutter 2018; Wang, Xu, and Wang 2018; Bertrand et al. 2017) and also referred to as bracket warm starting. In more detail, HJ uses its models to identify which set of configurations maximize the EI when deployed using *full budget* — recall that, as in HB, our aim is to maximize accuracy using the full budget. This allows HJ to leverage prior knowledge, unlike HB, at no considerable extra cost, since no additional models are trained nor maintained.

3.5 Optimizations

HJ adopts two optimizations that aim, resp., at reducing the cost of evaluating configurations that were previously tested with lower budgets — *pause-resume training* — and increasing, at no extra cost, the information that can be fed to the model — *opportunistic evaluation*.

Pause-resume training. In a HB’s bracket, configurations are tested multiple times with increasing budget values. This technique takes advantage of this observation by saving the model obtained after evaluating a configuration c with budget b^\dagger , noted $\mathcal{M}(c, b^\dagger)$. If later on (in the same or in a different HJ bracket), c is tested again with a budget $b^* > b^\dagger$, HJ reloads $\mathcal{M}(c, b^\dagger)$ and resumes the training from there (thus reducing the “cost” of training by b^\dagger). Note that this optimization is not new in the context of hyper-parameter optimization, e.g., (Swersky, Snoek, and Adams 2014; Golovin et al. 2017; Liaw et al. 2018)

Opportunistic evaluation. In modern ML frameworks, (e.g., NNs trained using the parameter server approach (Li et al. 2014)), the model’s validation error is typically monitored (and made available) throughout the training process and not only upon its conclusion. We take advantage of this as follows. Assume that a configuration c , so far not tested with budget b^\dagger , is requested to be tested with budget $b^* > b^\dagger$ (e.g., when HJ jumps from the first to the last, say the fifth, stage). In such a case, during the evaluation of c with budget b^* , when the training process reaches budget b^\dagger we measure the model’s current accuracy, noted $acc(c, b^\dagger)$ and extend the models’ dataset with the observation $\langle c, b^\dagger, acc(c, b^\dagger) \rangle$, enriching its knowledge base in an *opportunistic* fashion, i.e., at no additional cost. To the best of our knowledge, this optimization has not yet been proposed in the literature.

3.6 Preserving HyperBand theoretical guarantees

An appealing theoretical property of HB is that its exploration policy is guaranteed to be at most a constant factor slower than random search. In order to preserve this property, HJ exploits two mechanisms: **i**) with probability p_{NJ} HJ is forced not to jump and abide by the original SH/HB logic; **ii**) when selecting the configurations to include in a bracket, a fraction p_U is selected uniformly at random (as in HB) and not using the model.

The former mechanism ensures that, independently of how model mispredictions affect HJ’s policy, there exists a non-null probability that HJ will not deviate from

the HB’s policy (by jumping) in any of the brackets that it executes. The latter mechanism, originally proposed in BOHB (Falkner, Klein, and Hutter 2018), ensures that, independently of the model’s behavior, every configuration has a non-null probability of being included in a bracket. We adopt as default value for p_U the same used by BOHB, i.e., 0.3, and use the same value also for p_{NJ} .

3.7 Parallelizing HyperJump

Existing approaches for parallelizing HB can be classified as either synchronous or asynchronous. In synchronous approaches (Li et al. 2018; Falkner, Klein, and Hutter 2018), the size of the stages abides by the original HB’s rules and parallelization can be achieved at the level of HB’s stage, bracket, and iteration. Asynchronous methods, like ASHA (Li et al. 2020) or Ray Tune (Liaw et al. 2018), conversely, consider a single logical bracket in which a configuration c is promoted to the next stage iff c is in the η^{-1} top configurations already tested in the current stage.

HJ can be straightforwardly parallelized using synchronous strategies. If parallelization is pursued at the level of brackets or iterations, each worker simply runs an independent instance of HJ that shares the same model and training set (so to share the knowledge acquired by the parallel HJ instances). When parallelizing the testing of the configurations in the same stage, as soon as a worker completes the testing of a configuration, the model can be updated and the risk of jumping computed. If a jump is performed, the workers that are still evaluating configurations in the current stage can either be immediately interrupted or allowed to complete their current evaluation. In our implementation, we opted for the former option, which has the advantage of maximizing the number of workers that are immediately available for testing configurations in the stage targeted by the jump.

In more detail, our implementation adopts the same parallelization strategy of BOHB, i.e., parallelizing by stage and activating a new parallel bracket in the presence of idle workers, with one exception. We prevent starting a new parallel bracket if there are idle workers during the first bracket. This, in fact, would reduce the available computational resources to complete the first bracket and, consequently, lead to a likely increase of the latency to recommend the first incumbent (i.e., to test a full budget configuration).

Investigating how to employ HJ in combination with asynchronous versions of HB is out of the scope of this paper. Yet, we argue that the key ideas at the basis of HJ could still be applied in this context, opening up an interesting line of future research. For instance, in ASHA, one could use a model-based approach, similar to the one employed by HJ, to: **(i)** promote by more than one position/budget the testing of a configuration that the model predicts to be promising; or **(ii)** use the model to determine whether it is actually beneficial to promote a given configuration, e.g., avoid promoting less promising configurations to save computational resources that may be soon required to evaluate more promising configurations.

4 Evaluation

This section evaluates HJ both in terms of the quality of the recommended configurations and of its optimization time. We compare HJ against 6 state-of-the-art optimizers using 6 benchmarks and considering both sequential and parallel deployments. We also perform an ablation study to dive into the performance of HJ’s different components.

Benchmarks. Firstly, we consider the (distributed) training of 3 different neural networks (NNs): a Convolutional Neural Network (CNN), a Multilayer Perceptron (MLP), and a Recurrent Neural Network (RNN). These networks were implemented using Tensorflow (Abadi et al. 2016) and trained on the MNIST data set (Deng 2012) in the AWS cloud. The hyper-parameter space is defined by 6 dimensions: batch size, learning rate, and training mode (sync. vs async.), as well as the number, type, and size of the virtual machines used for training. The VM-related search space dimensions are relevant in the search procedure as they impact the quality of the configurations (see, e.g., (Casimiro et al. 2020; Mendes et al. 2020)). This impact is discussed in more detail in the supplemental material.

This space was discretized and exhaustively explored off-line in order to identify the optimum. We used the data set produced via these experiments to benchmark HJ also in a neural architecture search (NAS) scenario, in which one seeks to optimize also the underlying NN architecture by selecting either a CNN, an MLP or an RNN.

Next, we consider Light UNET (Ronneberger, Fischer, and Brox 2015) (trained with the 2017 CCF BDCI data set). The hyper-parameter space spans the following 6 dimensions: batch size, learning rate, momentum, training mode, as well as the type and number of GPUs installed on the machine used for training. Also, in this case we discretized the search space and exhaustively sampled it by training the model in each configuration during 5 hours, and measuring its accuracy periodically.

Finally, we use LIBSVM (Chang and Lin 2011) on the Covertype data set (Dua and Graff 2017), which we sub-sampled by $\approx 5 \times$ due to time and hardware constraints. The considered hyper-parameters are the kernel (linear, polynomial, RBF, and sigmoid), γ , and C . In this case we could not exhaustively explore off-line the hyper-parameter space, so the optimum is unknown. Since LIBSVM does not support pause-resume training and does not output the model’s accuracy during the intermediate phases of training, with this benchmark we cannot exploit the optimizations presented in Sec. 3.5. Additional details on these benchmarks are provided in the supplemental material.

Baselines and experimental setup. We compare HJ against six optimizers: HB, BOHB, ASHA, Fabolas, standard BO with EI, and Random Search (RS). The last two techniques (EI and RS) evaluate configurations only with the full-budget. The implementation of HJ extends the publicly available code of BOHB, which also provides an implementation of HB. ASHA was implemented by extending the same framework. To evaluate Fabolas, we used its publicly available implementation provided by the authors.

We use the default parameters of BOHB and Fabolas. To test HJ in a broader range of settings, we consider two different values of the η parameter: 2 for CNN, NAS and UNET; 3 for the others. For fairness, when comparing HJ, HB, BOHB, and ASHA, we configure them to use the same η value. We use the default value of 10% for the threshold λ for HJ and include in the supplemental material a study on the sensitivity to the tuning of λ . We use time as the budget in RNN, MLP and UNET, and training set size for the remaining benchmarks. The reported results represent the average over 30 independent runs.

Sequential deployment. Figure 1 reports the average loss (and corresponding standard deviation in the shaded areas) as a function of the wall clock time (i.e., training and recommendation time) for the considered benchmarks. We start by analyzing the plots in the first two rows, which refer to a sequential deployment scenario, i.e., a single worker is available for evaluating configurations. We do not include in this study ASHA, since ASHA is optimized for parallel deployments. For space constraints we report the results for NAS in the supplemental material, but they show similar trends.

In all the benchmarks, HJ provides significant speed-ups with respect to all the baselines to identify both configurations of good quality as well as near optimal ones. The largest speed-ups for recommending good quality solutions are achieved in CNN, UNET, RNN, and SVM, where the gains of HJ w.r.t. the best baseline range from around $20 \times$ to $10 \times$. As for identifying close to optimum configurations, the largest speed-ups against the best baseline are achieved in RNN ($\approx 10 \times$), CNN ($\approx 5 \times$) and UNET ($\approx 2.5 \times$).

In our benchmarks, BOHB provides marginal benefits when compared to HB. As we show in the supplemental material, this is imputable to the limited accuracy of the modelling approach used by BOHB (based on TPE and on a model per budget) which, albeit fast, is not very effective in identifying high quality configurations to include in a new bracket. Fabolas’ performance is hindered by its large recommendation times, which are already on the order of a few minutes in the early stages of the optimization and grow more than linearly: as a consequence, Fabolas suffers from large overheads especially with benchmarks that have shorter training times (e.g. RNN) and, across all benchmarks, in the initial phase of the optimization process (where HJ, BOHB and HB, can evaluate several configurations by the time Fabolas produces its first recommendation). Finally, the limitations of EI, which only uses full-budget sampling, are particularly clear with SVM. Here, training times grow more than linearly with the training set size, which is the budget used by the multi-fidelity optimizers, thus amplifying the speed-ups achievable by using low-fidelity observations w.r.t. the other benchmarks.

Ablation study. Figure 1f shows the result of an ablation study aimed at quantifying the contributions of the various mechanisms employed by HJ. We report the performance obtained on UNET by four HJ variants obtained by disabling each of the following mechanisms: **(i)** the pause-resume training and opportunistic evaluation optimizations (HJ-no-Opt); **(ii)** warm-starting the bracket (HJ-no-BW); **(iii)** prior-

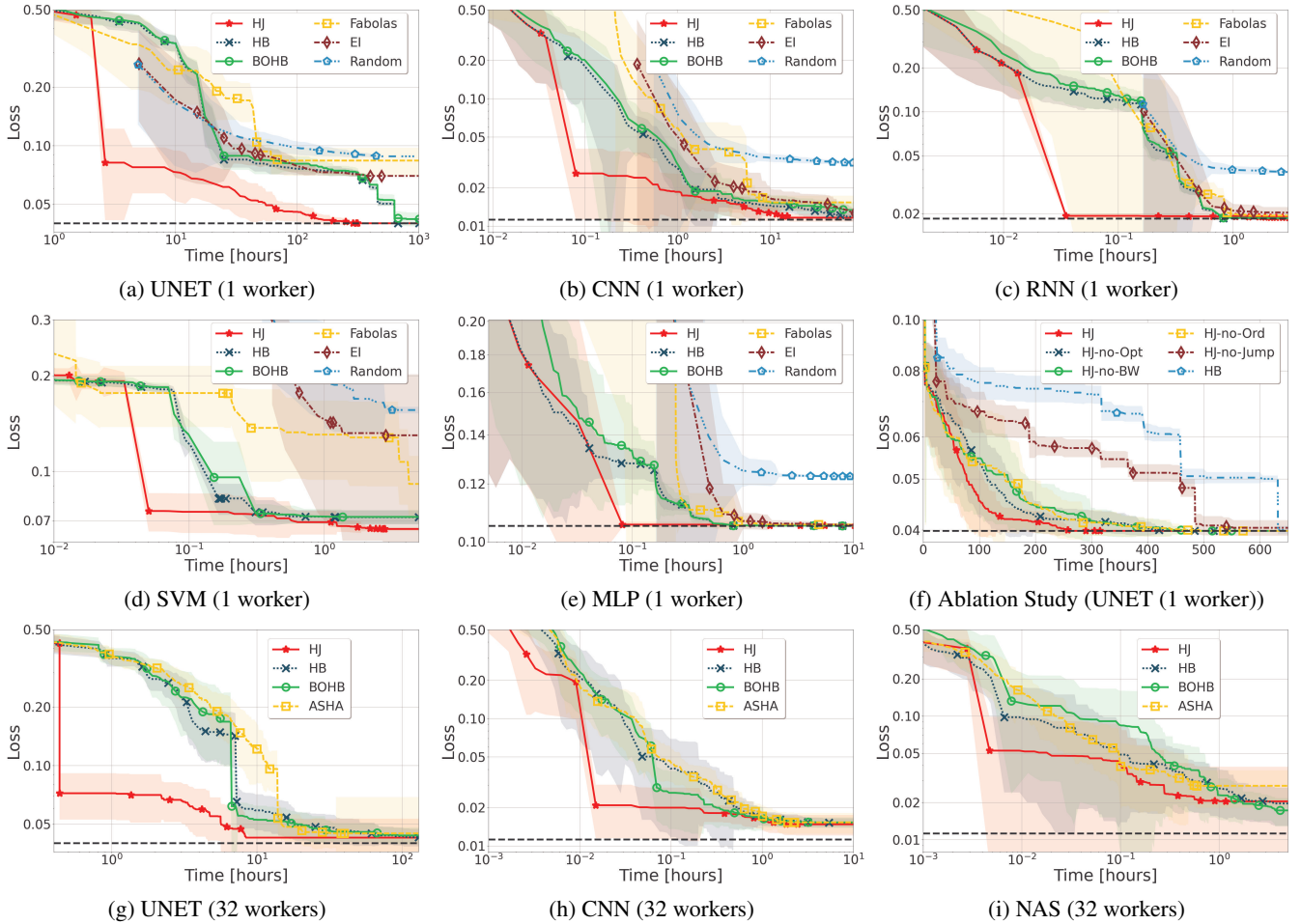


Figure 1: Comparison of HJ against other state-of-the-art optimizers in sequential and parallel deployments. Plot (f) reports an ablation study for HJ. The dashed horizontal line indicates the optimum (when it is known).

itizing the evaluation order of configurations (HJ-no-Ord); **(iv)** the jumping logic (HJ-no-Jump). We include in the plot also HB, which can be regarded as a variant of HJ from which we disabled all of the mechanisms proposed in this paper. This data shows that the first three of these mechanisms have a similar impact on the performance of HJ: disabling any of them increases the time required by HJ to identify the optimum by nearly 40%; a similar slow-down factor can be observed also throughout the optimization process, e.g., the time taken to reach a loss of 5% is around 40% larger with HJ-no-Opt and around 80% larger with HJ-no-BW and HJ-no-Ord. Further, the largest performance penalty is observed when disabling jumping, which confirms that this mechanism is indeed the one that most contributes to HJ’s efficiency.

Parallel Deployment. The third row of Fig. 1 reports the results when using a pool of 32 workers with UNET, CNN and NAS. The supplemental material includes the plots for the other benchmarks, as well as for a scenario with 8 workers. These data show that HJ achieves gains similar to (or even larger) than the ones previously observed, which con-

firms the competitiveness of HJ also in parallel deployments.

Recommendation overhead. We conclude by reporting experimental data regarding the computational overhead incurred by HJ to recommend the next configuration to test. The average recommendation time for HJ across all benchmarks is approx. 1.08 secs. This time includes model training, determining whether to jump and the next configuration to test in the current stage, and, overall, confirms the computational efficiency of the proposed approach.

5 Conclusions

This paper introduced HyperJump, a new approach that complements HyperBand’s robust search strategy and accelerates it by skipping low risk evaluations. HJ’s efficiency hinges on the synergistic use of several innovative risk modelling techniques and of a number of pragmatic optimizations. We show that HJ provides over one-order of magnitude speed-ups on a variety of deep-learning and kernel-based learning problems when compared to HB as well as to a number of state of the art optimizers.

References

Abadi, M.; et al. 2016. TensorFlow: A System for Large-scale Machine Learning. In *Proceedings of OSDI '16: 12th USENIX Symposium on Operating Systems Design and Implementation*.

Bergstra, J.; Bardenet, R.; Bengio, Y.; and Kégl, B. 2011. Algorithms for Hyper-Parameter Optimization. In *Advances in Neural Information Processing Systems*, volume 24, 2546–2554. Curran Associates, Inc.

Bertrand, H.; Ardon, R.; Perrot, M.; and Bloch, I. 2017. Hyperparameter optimization of deep neural networks: combining Hyperband with Bayesian model selection. In *Proceedings of Conférence sur l'Apprentissage Automatique*.

Breiman, L. 2001. Random Forests. *Machine Learning*, 45(1).

Brochu, E.; Cora, V. M.; and de Freitas, N. 2010. A Tutorial on Bayesian Optimization of Expensive Cost Functions, with Application to Active User Modeling and Hierarchical Reinforcement Learning. Technical Report arXiv:1012.2599.

Casimiro, M.; Didona, D.; Romano, P.; Rodrigues, L.; Zwanepoel, W.; and Garlan, D. 2020. Lynceus: Cost-efficient Tuning and Provisioning of Data Analytic Jobs. In *Proceedings 20th IEEE International Conference on Distributed Computing Systems*.

Chang, C.-C.; and Lin, C.-J. 2011. LIBSVM: A Library for Support Vector Machines. *ACM Transactions on Intelligent Systems and Technology*, 2.

Dai, Z.; Yu, H.; Low, B. K. H.; and Jaitlet, P. 2019. Bayesian Optimization Meets Bayesian Optimal Stopping. In *Proceedings of the 36th International Conference on Machine Learning*, volume 97.

Deng, L. 2012. The MNIST database of handwritten digit images for machine learning research [Best of the Web]. In *IEEE Signal Processing Magazine*, volume 29. IEEE.

Domhan, T.; Springenberg, J. T.; and Hutter, F. 2015. Speeding up Automatic Hyperparameter Optimization of Deep Neural Networks by Extrapolation of Learning Curves. In *Proceedings of the 24th International Joint Conference on Artificial Intelligence*.

Dua, D.; and Graff, C. 2017. UCI Machine Learning Repository.

Falkner, S.; Klein, A.; and Hutter, F. 2018. BOHB: Robust and Efficient Hyperparameter Optimization at Scale. In *Proceedings of the 35th International Conference on Machine Learning*, volume 80.

Golovin, D.; Solnik, B.; Moitra, S.; Kochanski, G.; Karro, J.; and Sculley, D. 2017. Google Vizier: A Service for Black-Box Optimization. In *Proceedings of the 23rd ACM SIGKDD International Conference on Knowledge Discovery and Data Mining*.

Jamieson, K.; and Talwalkar, A. 2016. Non-stochastic best arm identification and hyperparameter optimization. In *Proceedings of the 19th International Conference on Artificial Intelligence and Statistics*.

Klein, A.; Falkner, S.; Bartels, S.; Hennig, P.; and Hutter, F. 2017. Fast Bayesian Optimization of Machine Learning Hyperparameters on Large Datasets. In *Proceedings of the 20th International Conference on Artificial Intelligence and Statistics*, volume 54.

Klein, A.; Tiao, L. C.; Lienart, T.; Archambeau, C.; and Seeger, M. 2020. Model-based asynchronous hyperparameter and neural architecture search. *arXiv preprint arXiv:2003.10865*.

Lam, R.; and Willcox, K. 2017. Lookahead Bayesian Optimization with Inequality Constraints. In *Proceedings of the 31st International Conference on Neural Information Processing Systems*.

Lam, R. R.; Willcox, K. E.; and Wolpert, D. H. 2016. Bayesian Optimization with a Finite Budget: An Approximate Dynamic Programming Approach. In *Proceedings of the 29th Neural Information Processing Systems Conference*.

Li, L.; Jamieson, K.; DeSalvo, G.; Rostamizadeh, A.; and Talwalkar, A. 2018. Hyperband: A novel bandit-based approach to hyperparameter optimization. *Journal of Machine Learning Research*, 18: 1–52.

Li, L.; Jamieson, K.; Rostamizadeh, A.; Gonina, E.; Bentzur, J.; Hardt, M.; Recht, B.; and Talwalkar, A. 2020. A System for Massively Parallel Hyperparameter Tuning. In Dhillon, I.; Papailiopoulos, D.; and Sze, V., eds., *Proceedings of Machine Learning and Systems*, volume 2, 230–246.

Li, M.; Andersen, D. G.; Park, J. W.; Smola, A. J.; Ahmed, A.; Josifovski, V.; Long, J.; Shekita, E. J.; and Su, B.-Y. 2014. Scaling Distributed Machine Learning with the Parameter Server. In *Proceedings of the 11th USENIX Conference on Operating Systems Design and Implementation*.

Liaw, R.; Liang, E.; Nishihara, R.; Moritz, P.; Gonzalez, J. E.; and Stoica, I. 2018. Tune: A Research Platform for Distributed Model Selection and Training. *arXiv preprint arXiv:1807.05118*.

Mendes, P.; Casimiro, M.; Romano, P.; and Garlan, D. 2020. TrimTuner: Efficient Optimization of Machine Learning Jobs in the Cloud via Sub-Sampling. In *2020 28th International Symposium on Modeling, Analysis, and Simulation of Computer and Telecommunication Systems*. IEEE.

Mockus, J.; Tiesis, V.; and Zilinskas, A. 1978. The Application of Bayesian Methods for Seeking the Extremum. In *Toward Global Optimization*, volume 2, 117–128. Elsevier.

Rasmussen, C. E.; and Williams, C. K. 2006. *Gaussian Processes for Machine Learning*. Cambridge, MA, USA: MIT Press.

Ronneberger, O.; Fischer, P.; and Brox, T. 2015. U-Net: Convolutional Networks for Biomedical Image Segmentation. In *Medical Image Computing and Computer-Assisted Intervention – MICCAI 2015*. Springer International Publishing.

Snoek, J.; Larochelle, H.; and P. Adams, R. 2012. Practical Bayesian Optimization of Machine Learning Algorithms. In *Proceedings of the 25th International Conference on Neural Information Processing Systems*, volume 2.

Swersky, K.; Snoek, J.; and Adams, R. P. 2013. Multi-task Bayesian Optimization. In *Proceedings of the 26th International Conference on Neural Information Processing Systems*, volume 2.

Swersky, K.; Snoek, J.; and Adams, R. P. 2014. Freeze-thaw bayesian optimization. *arXiv preprint arXiv:1406.3896*.

Wang, J.; Xu, J.; and Wang, X. 2018. Combination of Hyperband and Bayesian Optimization for Hyperparameter Optimization in Deep Learning. *arXiv preprint arXiv:1406.3896*.

Yue, X.; and Kontar, R. A. 2020. Why Non-myopic Bayesian Optimization is Promising and How Far Should We Look-ahead? A Study via Rollout. *arXiv preprint arXiv:1911.01004*.

Supplementary Material for HyperJump: Accelerating HyperBand via Risk Modelling

Pedro Mendes^{1,2}, Maria Casimiro^{1,2}, Paolo Romano¹

¹*INESC-ID and Instituto Superior Técnico, Universidade de Lisboa*

²*Institute for Software Research, Carnegie Mellon University*

{pgmendes, mdaloura}@andrew.cmu.edu, romano@inesc-id.pt

This document provides additional details about different aspects of HyperJump, a novel hyper-parameter optimization method that builds upon HB’s robust search strategy and accelerates it via an innovative, model-based technique. Specifically, this document is organized as follows:

- **Section 1** provides details about the custom GP kernel employed by HJ to predict the quality of untested configurations.
- **Section 2** discusses how the equations for computing the Expected Accuracy Reduction (EAR) can be mathematically derived and numerically computed.
- **Section 3** provides details on the heuristic employed to select the candidate sets of configurations for a jump.
- **Section 4** details the pseudo-code for the heuristic used to select the next configurations to evaluate in a stage.
- **Section 5** details the benchmarks used to evaluate HJ.
- **Section 6** discusses the implementation of the software used to evaluate HJ and provides information on how it can be obtained.
- **Section 7** presents additional experimental results in which we compare HyperJump to several state-of-the-art approaches.
- **Section 8** presents a study that evaluates the impact of tuning the risk threshold λ on the performance of HJ.
- **Section 9** evaluates the benefits of the strategy for bracket warm starting used in HJ.

1 Models used to predict the quality of untested configurations

This section provides additional details on the models used by HJ to predict the quality of untested configurations. As already mentioned (see Section 3.1 of the main body paper), in our implementation of HJ we opted for GPs as underlying black-box modelling toolkit, as GPs are among the most popular modelling technique used in the literature of BO. Note though that, in principle, alternative modelling techniques could be exploited (e.g., an ensemble of GPs (Breiman 1996, 2001) or Adaptive Bayesian linear regression (Valkov et al. 2018)) provided that they can not only

predict the mean value but also estimate the predictions’ uncertainty via a Gaussian distribution.

Similarly to recent related works (Klein et al. 2017, 2020; Mendes et al. 2020), we include in the feature space of the GP models not only the hyper-parameters’ space, but also the budget (so as to enable inter-budget extrapolation). Further, analogously to, e.g., (Klein et al. 2017; Mendes et al. 2020), we employ a custom Bayesian Linear Kernel that encodes the expectation that the loss function has an exponential decay with larger budgets, along with a generic Matérn 5/2 kernel that is used to capture relations among the hyper-parameters. More in detail, we normalized each dimension of the search space, and decided to model the loss (instead of accuracy). Thus, all the dimensions associated to the hyper-parameters to be optimized use the Matérn 5/2 kernel (Matérn 1986). The basis function used to capture variations of the budget is instead defined as:

$$\phi(b^*) = (1, (1 - b^*)^2)^T$$

Note that we normalized each dimension, thus $b^* \in [0, 1]$.

Finally, also similarly to prior work, e.g., (Falkner, Klein, and Hutter 2018), we start using the model (and enable HJ’s jumping logic) only after having gathered at least $d+2$ observations, where d is the number of dimensions of the hyper-parameter space.

2 Computing the Expected Accuracy Reduction

This section provides details on how to compute the Expected Accuracy Reduction (EAR). Recall that the EAR of a jump from stage s to stage $s + 1$ in which we discard the configurations in \mathcal{D} and select the ones in \mathcal{S} is defined as:

$$\begin{aligned} EAR_s^{s+1}(\mathcal{D}, \mathcal{S}) &= \int_{-\infty}^{+\infty} P(\mathcal{A}_s^{\mathcal{D}} - \mathcal{A}_s^{\mathcal{S}} = x) \max\{\mathcal{A}_s^{\mathcal{D}} - \mathcal{A}_s^{\mathcal{S}}, 0\} dx \\ &= \int_0^{+\infty} x P(\mathcal{A}_s^{\mathcal{D}} - \mathcal{A}_s^{\mathcal{S}} = x) dx \end{aligned} \quad (1)$$

where we have noted with $\mathcal{A}_s^{\mathcal{D}} = \max_{c_i \in \mathcal{D}} A(c_i, b_s)$, $\mathcal{A}_s^{\mathcal{S}} = \max_{c_k \in \mathcal{S}} A(c_k, b_s)$, and $b_s = b\eta^s$.

Before discussing how to compute Eq. (1), let us detail how to compute the PDF of $\mathcal{A}_s^{\mathcal{D}}$ and $\mathcal{A}_s^{\mathcal{S}}$.

Let \mathcal{T} be an arbitrary subset of the configurations in stage s . We use the notation $\phi_{\mathcal{A}_s^{\mathcal{T}}}(x)$ and $\Phi_{\mathcal{A}_s^{\mathcal{T}}}(x)$ to refer to the PDF and CDF, respectively, of $\mathcal{A}_s^{\mathcal{T}}$. We distinguish three cases: (1) \mathcal{T} contains only tested configurations that have been evaluated via noise-free measurements; (2) \mathcal{T} contains only untested configurations or configurations tested via noisy measurements; (3) \mathcal{T} contains some configurations tested via noise-free measurements and configurations that are either untested or tested via noisy measurements

Let us start by considering the first case, i.e., \mathcal{T} only contains configurations tested via noise-free measurements, such that all configurations in \mathcal{T} are described by a Dirac δ function. In this case, the PDF of $\mathcal{A}_s^{\mathcal{T}}$ is simply:

$$\phi_{\mathcal{A}_s^{\mathcal{T}}}(x) = \delta(x - \max_{c_i \in \mathcal{T}} A(c_i, b_s)) \quad (2)$$

If \mathcal{T} only contains untested configurations or if the tested configurations are subject to noisy measurements, then the accuracy predictions for any configuration in \mathcal{T} follow a normal distribution. The CDF of $\mathcal{A}_s^{\mathcal{T}}$, noted $\Phi_{\mathcal{A}_s^{\mathcal{T}}}$, can then be computed in closed form as the product of the CDFs of the normal distributions associated with the configurations $c \in \mathcal{T}$, i.e., $\Phi_{A(c, b_s)}$:

$$\Phi_{\mathcal{A}_s^{\mathcal{T}}}(x) = \prod_{c \in \mathcal{T}} \Phi_{A(c, b_s)}(x) = \prod_{c \in \mathcal{T}} \Phi\left(\frac{x - \mu_{A(c, b_s)}}{\sigma_{A(c, b_s)}}\right) = \exp\left(\sum_{c \in \mathcal{T}} \log \Phi\left(\frac{x - \mu_{A(c, b_s)}}{\sigma_{A(c, b_s)}}\right)\right), \quad (3)$$

where we have denoted with $\Phi(x)$ the CDF of the standard normal distribution and with $\mu_{A(c, b_s)}$, $\sigma_{A(c, b_s)}$ the average and standard deviation of the predicted accuracy of c with budget b_s , respectively. Then, we can determine the PDF by computing the derivative of the CDF:

$$\phi_{\mathcal{A}_s^{\mathcal{T}}}(x) = \frac{d}{dx} \Phi_{\mathcal{A}_s^{\mathcal{T}}}(x) = \prod_{c \in \mathcal{T}} \Phi\left(\frac{x - \mu_{A(c, b_s)}}{\sigma_{A(c, b_s)}}\right) \cdot \sum_{c \in \mathcal{T}} \frac{\phi\left(\frac{x - \mu_{A(c, b_s)}}{\sigma_{A(c, b_s)}}\right)}{\sigma_{A(c, b_s)} \Phi\left(\frac{x - \mu_{A(c, b_s)}}{\sigma_{A(c, b_s)}}\right)} \quad (4)$$

where $\phi(x)$ is the PDF of the standard normal distribution.

Finally, let us consider the case in which \mathcal{T} contains both configurations associated with Gaussian distributions (i.e., untested configurations or tested via noisy measurements) and configurations associated with Dirac δ functions (i.e., tested via noise-free measurements). Let us denote with \mathcal{T}_{δ} and $\mathcal{T}_{\mathcal{N}}$ the former and latter subset of configurations of \mathcal{T} , respectively. The PDF of $\mathcal{A}_s^{\mathcal{T}}$ is then given by

$$\phi_{\mathcal{A}_s^{\mathcal{T}}}(x) = H(x - \max_{c_i \in \mathcal{T}_{\delta}} A(c_i, b_s)) \frac{\phi_{\mathcal{A}_s^{\mathcal{T}_{\mathcal{N}}}}(x)}{P_{\mathcal{A}_s^{\mathcal{T}_{\mathcal{N}}}}(x \geq \max_{c_i \in \mathcal{T}_{\delta}} A(c_i, b_s))} \quad (5)$$

where H is the Heaviside function and $\phi_{\mathcal{A}_s^{\mathcal{T}_{\mathcal{N}}}}(x)$ can be computed using Eq. (4).

Algorithm 1: Pseudo-code of the logic used to determine the sets of configurations to consider when jumping from stage s to stage $s + 1$ (function `GET_CANDIDATES_FOR_S()`)

```

Set<Set<Config>> GET_CANDIDATES_FOR_S(Set<Config> Tested, Set<Config> Untested, int s)
1: Set<Set<Config>> O ← ∅ ▷ Set of selected safest sets to be returned
2: Set<Config> C ← Tested ∪ Untested ▷ C stores all the configs in current stage
3: Set<Config> K ← C.sortByAccuracy().getTop(|C|/η)
4: ▷ K stores the configs. with best (pred. or measured) accuracy
5: Set<Config> E ← C \ K
6: ▷ E stores the configs. with worse (pred. or measured) accuracy
7: O.add(K) ▷ Set K is one of the 1 + 2 $\lfloor \log_2 |\mathcal{K}| \rfloor$  recommended sets
8: ▷ Generate sets based on accuracy
9: for i in  $[1 \leq i \leq \lfloor \log_2 |\mathcal{K}| \rfloor]$  do
10:   Set X ← clone(K)
11:   ▷ Remove from K the  $|\mathcal{K}|/\eta^i$  configurations with worse accuracy...
12:   X.sortByAccuracy().removeBottom( $|\mathcal{K}|/\eta^i$ )
13:   ▷ ...and add the  $|\mathcal{K}|/\eta^i$  configurations with best accuracy from C \ K
14:   X.add(E.sortByAccuracy().getTop( $|\mathcal{K}|/\eta^i$ ))
15:   O.add(X)
16: end for ▷ Generate sets based on lower and upper confidence bounds
17: for i in  $[1 \leq i \leq \lfloor \log_2 |\mathcal{K}| \rfloor]$  do
18:   Set X ← clone(K)
19:   ▷ Remove from K the  $|\mathcal{K}|/\eta^i$  configurations with worse LCB
20:   X.sortByLCB().removeBottom( $|\mathcal{K}|/\eta^i$ )
21:   ▷ ...and add the  $|\mathcal{K}|/\eta^i$  configurations with best UCB from C \ K
22:   X.add(E.sortByUCB().getTop( $|\mathcal{K}|/\eta^i$ ))
23:   O.add(X)
24: end for
25: return O

```

Let us now discuss how to compute Eq. (1). The distribution $Z = \mathcal{A}_s^{\mathcal{D}} - \mathcal{A}_s^{\mathcal{S}} = X + Y$ can be computed as the convolution between two random variables X and Y .

$$f_Z(x) = f_X(x) * f_Y(y) = \int_{-\infty}^{+\infty} f_X(k) f_Y(x - k) dk. \quad (6)$$

Hence, Eq. (1) can be computed as:

$$EAR_s^{s+1}(\mathcal{D}, \mathcal{S}) = \int_0^{+\infty} \int_{-\infty}^{+\infty} f_X(k) f_Y(k - x) x dk dx, \quad (7)$$

where f_X and f_Y are obtained by Eq. (4). As an optimization, we take advantage of the existence of tested configurations with noise-free measurements (i.e., associated with Dirac δ functions) in \mathcal{S} and/or \mathcal{D} to simplify Eq. (7) as follows.

If all the configurations in \mathcal{S} are associated with a Dirac δ function and the configurations in \mathcal{D} are all associated with normal distributions, then Eq. (1) can be rewritten as follows:

$$EAR_s^{s+1}(\mathcal{D}, \mathcal{S}) = \int_0^{+\infty} [f_X(x) * f_Y(x)] x dx = \int_0^{+\infty} f_X(x + \max_{c_i \in \mathcal{S}} A(c_i, b_s)) x dx, \quad (8)$$

where f_Y is given by Eq. (2) and $f_X(x)$ by Eq. (4).

Analogously, if all the configurations in \mathcal{D} are tested and modelled by a Dirac δ function (i.e., f_X is determined using Eq. (2) and \mathcal{S} contains only configurations associated

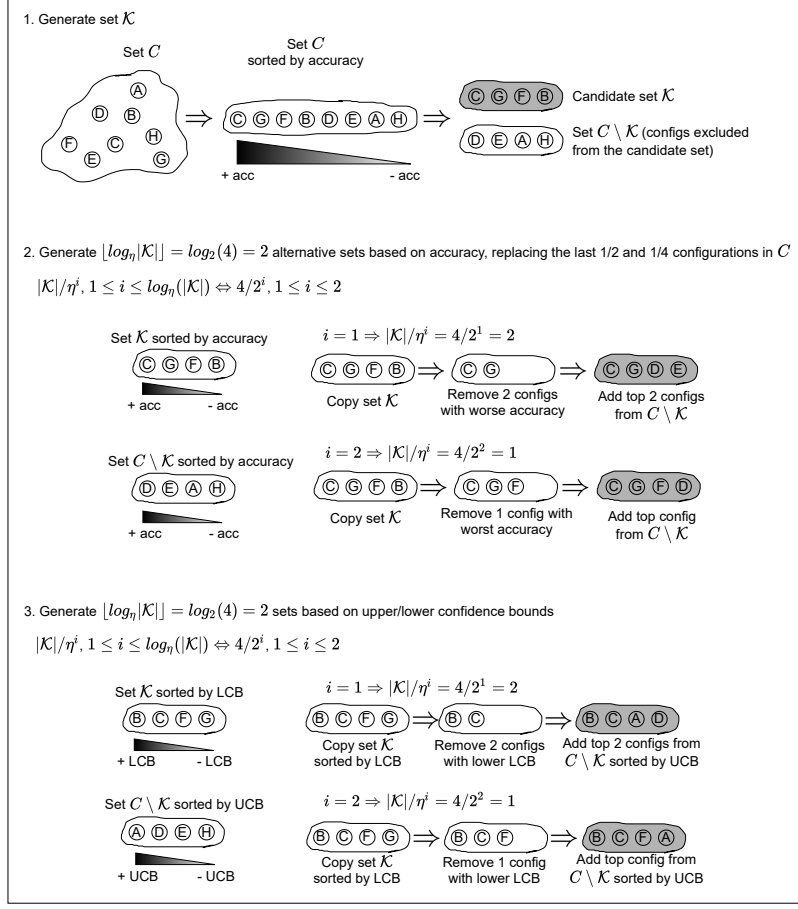


Figure 1: Illustration of the execution of the `GET_CANDIDATES_FOR_S` function, introduced in Section 3.2 of the main body of the paper. This function is used to determine the alternative sets of configurations to consider for a jump from stage s to $s + 1$. The alternative sets are highlighted in grey.

with normal distributions (i.e., $f_Y(x)$ is determined using Eq. (4)), the EAR can be computed as:

$$EAR_s^{s+1}(\mathcal{D}, \mathcal{S}) = \int_0^{+\infty} f_Y(-x + \max_{c_i \in \mathcal{D}} A(c_i, b_s)) x \, dx \quad (9)$$

Finally, in case only some (but not all) of the configurations in \mathcal{D} or \mathcal{S} are associated with a Dirac δ function, Eq. (7) can be simplified by reducing the interval of integration of the convolution due to the computation of the Heaviside function. For example, if both sets have tested and untested configurations, the EAR can be simplified by

$$EAR_s^{s+1}(\mathcal{D}, \mathcal{S}) = \int_0^{+\infty} \int_M^{+\infty} \frac{\phi_{\mathcal{A}_s^{\mathcal{D}, \mathcal{N}}}(k)}{P_{\mathcal{A}_s^{\mathcal{D}, \mathcal{N}}}(k \geq \max_{c_i \in \mathcal{D}_\delta} A(c_i, b_s))} \cdot \frac{\phi_{\mathcal{A}_s^{\mathcal{S}, \mathcal{N}}}(k - x)}{P_{\mathcal{A}_s^{\mathcal{S}, \mathcal{N}}}(k - x \geq \max_{c_i \in \mathcal{S}_\delta} A(c_i, b_s))} \, x \, dk \, dx \quad (10)$$

where $M = \max\{ \max_{c_i \in \mathcal{D}_\delta} A(c_i, b_s); x + \max_{c_i \in \mathcal{S}_\delta} A(c_i, b_s) \}$

Note that, although the PDF and the CDF of X and Y are known in closed form, the convolution can not be computed

analytically (and, as such, neither can Eq. (1)). Therefore, we need to resort to numerical methods to compute the convolution and determine the distribution Z and the respective expected value. Those were implemented in Python3.6 using the function `nquad` of the `scipy` package. Moreover, for efficiency reasons, we implemented in C the function to integrate that is called via the `LowLevelCallable` function. We use the default configuration values of `nquad`, except for the absolute error tolerance (which we set to 1^{-12}) and the upper bound on the number of sub-intervals used in the adaptive algorithm (which we set to 2500).

3 Determining the candidate sets of configurations targeted by a jump

In this section we provide additional details on the logic used by HJ to determine the sets of configurations to be considered when jumping from stage s to stage $s + 1$. This logic was already informally described in Section 3.2 and is used by Algorithm 2 (in the main body of the paper) where it is encapsulated into the function `GET_CANDIDATES_FOR_S`. In Algorithm 1 of this supplemental material, we report the

Algorithm 2: Pseudo-code of the mechanism used to select the next configuration to test in a stage (function NEXT_CONF_TO_TEST()).

```

Set<Config,risk> NEXT_CONF_TO_TEST(Set<Config> Untested, Set<Config> Tested,
int s)
1: Set<Config,risk> C=∅
2: for  $x \in$  Untested do
3:    $\triangleright$  Use GP model to predict accuracy of an untested configuration  $x$ ,
4:   acc = model.predictedAccuracy( $x, b\eta^s$ )
5:    $T^* = \text{Tested} \cup \{(x, acc)\}$ ;  $U^* = \text{Untested} \setminus \{x\}$ 
6:    $\triangleright$  Estimate the risk of jumping after emulating testing  $x$  via the model
7:   risk = EVALUATE_JUMP_RISK( $s, T^*, U^*$ ).getJumpRisk()
8:    $C = C \cup \langle x, \text{risk} \rangle$ 
9: end for
10:   $\triangleright$  Return the (untested) configuration with minimum estimated risk
11: return  $x$  s.t.  $\langle x, \text{risk} \rangle \in C \wedge \forall \langle y, \text{risk}' \rangle \in C : \text{risk}' \geq \text{risk}$ 

```

pseudo-code formalizing the logic of this function. In order to further clarify the logic of this function we also exemplify its execution in Figure 1.

4 Selecting the next configurations to evaluate in a stage

Algorithm 2 reports the pseudo-code of the NEXT_CONF_TO_TEST() function, which is responsible for determining the next configuration to test in the current stage. The logic of this function was described in Section 3.3 of the main body of the paper.

5 Benchmarks

This section provides additional details on the benchmarks that we used to evaluate HyperJump. Firstly, we deployed in the AWS cloud the distributed training of 3 different neural networks (NNs): a Convolutional Neural Network (CNN), a Multilayer Perceptron (MLP), and a Recurrent Neural Network (RNN). We consider a parameter space composed of 6 dimensions: batch size, learning rate, and training mode, as well as the number, type, and size of the virtual machines used for training. This space was discretized and the considered values are resumed in Table 1.

Table 1: Hyper- and cloud parameters.

Parameter	Values	
Learning rate	$\{10^{-3}, 10^{-4}, 10^{-5}\}$	
Batch size	$\{16, 256\}$	
Training mode	$\{\text{sync, async}\}$	
VM type	VM characteristics	#VMs
t2.small	$\{1 \text{ vCPU, 2 GB}\}$	$\{8, 16, 32, 48, 64, 80\}$
t2.medium	$\{2 \text{ vCPU, 4 GB}\}$	$\{4, 8, 16, 24, 32, 40\}$
t2.xlarge	$\{4 \text{ vCPU, 16 GB}\}$	$\{2, 4, 8, 12, 16, 20\}$
t2.2xlarge	$\{8 \text{ vCPU, 32 GB}\}$	$\{1, 2, 4, 6, 8, 10\}$

We trained the NNs using the MNIST data set (Deng 2012) with 60000 images to train and 10000 images to test the NN. We trained in each of the different configurations

Table 2: UNET hyper- and hardware parameters.

Parameter	Values
Learning rate	$\{10^{-4}, 10^{-5}, 10^{-6}\}$
Batch size	$\{1, 2\}$
Momentum	$\{0.9, 0.95, 0.99\}$
Training mode	$\{\text{sync, async}\}$
GPU type	#GPUs
GeForce GTX 1080	$\{1, 2\}$
GeForce RTX 2080 Super	$\{1, 2\}$

Table 3: SVM hyper-parameters.

Parameter	Values
Kernel	{linear, polynomial deg. 2, polynomial deg. 3, polynomial deg. 4, RBF, Sigmoid}
Gamma	$\{1e-6, 1e-5, 1e-4, 1e-3, 5e-3, 1e-2, 5e-3, 0.1, 0.5, 1, 2.5, 7, 10, 20, 30, 40, 50, 60, 70, 80, 90, 100\}$
C	$\{1e-6, 1e-5, 1e-4, 1e-3, 5e-3, 1e-2, 5e-3, 0.1, 0.5, 1, 2.5, 7, 10, 20, 30, 40, 50, 60, 70, 80, 90, 100\}$

using 5 different sub-sampled data sets and also measured the model’s validation loss periodically. We set an additional timeout to stop the training after 10 minutes in order to control and bound the cost to pay in the cloud. This is a common approach when the training of machine learning (ML) models is deployed in the cloud (Mendes et al. 2020; Casimiro et al. 2020).

We created a variant of the above benchmarks using the training time as budget, instead of data set size. This was done by considering as the full budget a 10 minutes training time; the intermediate time and accuracy values measured when training with the full data set were then used to derive the model’s accuracy at intermediate (time) budgets. We also extended both data sets produced via these experiments in order to benchmark HJ in a neural architecture search (NAS) scenario, in which we also optimize the NN architecture (CNN, MLP, or RNN) by adding an additional dimension to the search space corresponding to the architecture to use.

Note that we included in the search space not only the model’s hyper-parameters, but also type and number of virtual machines employed, since, as shown in prior work, e.g., (Zhang et al. 2016; Casimiro et al. 2020), the size and characteristics of the underlying computing infrastructure can have a strong impact on the efficiency of the worker’s synchronization and model convergence speed. More in detail, in both the above mentioned scenarios (dataset size or training time as budget) we rely on a parameter server architecture to train the NNs, either in a synchronous or asynchronous mode. In these settings the choice of the number of workers, once we fix the model’s hyper-parameters (in particular synchronous vs asynchronous training), can have a large impact on accuracy. In particular, when setting training time as budget, using more powerful machines intuitively yields higher accuracy with the same budget and

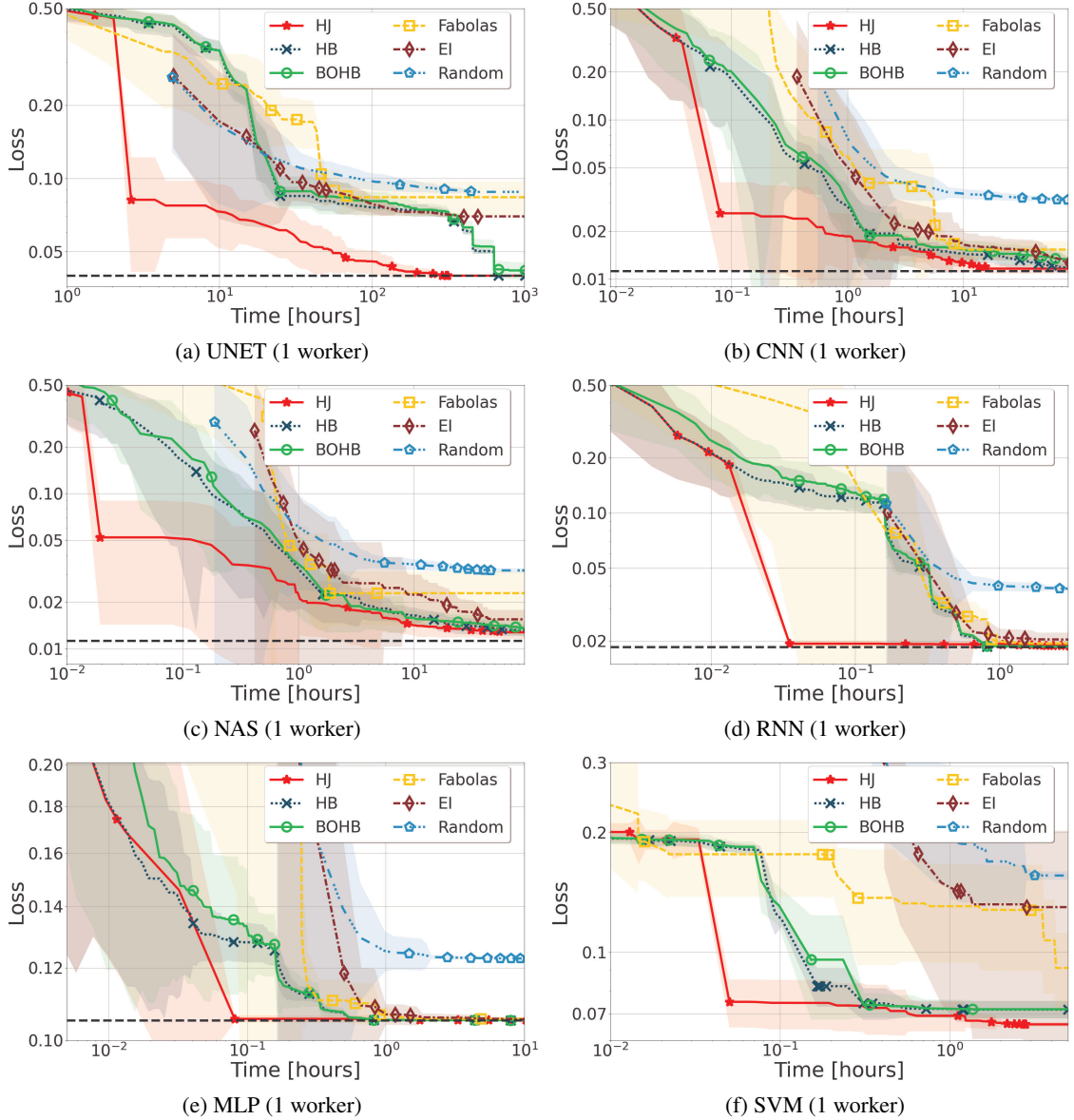


Figure 2: Comparison of HJ against other state-of-the-art optimizers in a sequential deployment scenario (1 worker).

hyper-parameter settings. As for the case of using dataset size as budget, we have experimentally observed that the model's accuracy varies significantly if we change the number and type of VMs over which we train the model, even using the same hyper-parameters. For instance, using a large number of machines with small datasets and high learning rates can cause the training procedure to become unstable (after an initial improvement, validation loss tends to degrade over time), whereas the model built using a single worker achieves a much higher accuracy.

Next, we considered Light UNET (Ronneberger, Fischer, and Brox 2015) (trained with the 2017 CCF BDCl data set). Also in this case the search space is composed of 6 dimensions/hyper-parameters (see Table 2): batch size,

learning rate, momentum, training mode, as well as the type and number of GPUs installed on the machine used for training. In this case we also discretized the search space and exhaustively sampled it by training the model in each configuration during 5 hours and measuring its accuracy periodically.

In all the benchmarks described so far, in order to reduce noise in the measurements, we trained each configuration three times, monitoring the model's accuracy periodically, and considered the average of these runs.

At last, we considered the training of a Support Vector Machine (SVM) implemented via the LIBSVM (Chang and Lin 2011) framework and trained on the Covertype data set (Dua and Graff 2017). Due to time and hardware constraints,

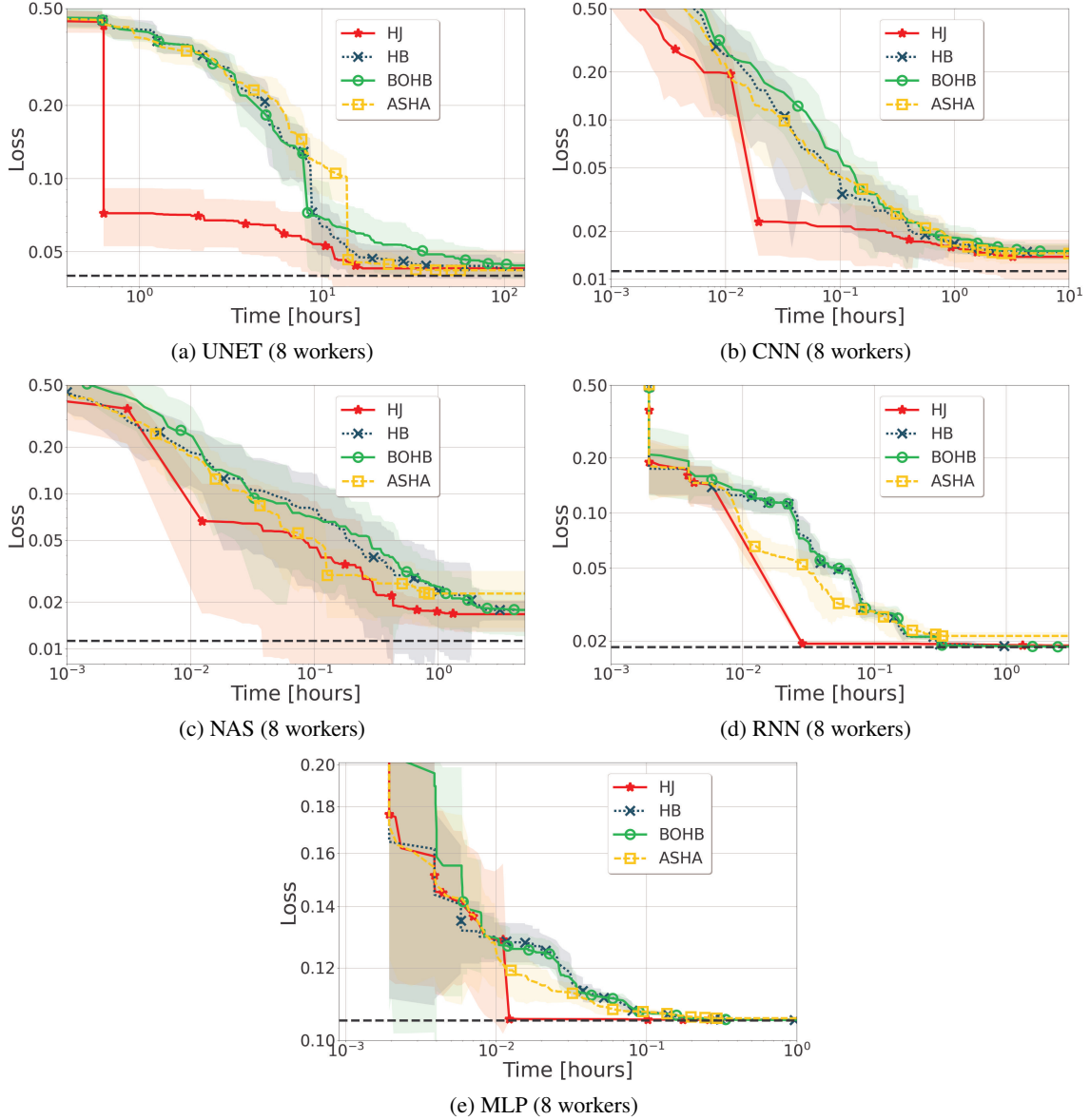


Figure 3: Comparison of HJ against other state of the art optimizers in a parallel deployment scenario using 8 workers.

we reduced the data set size by $\approx 5\times$. In this case, we considered a smaller number of dimensions (i.e., 3 dimensions) but a higher number of configurations. The considered hyper-parameters are the kernel (linear, polynomial with degree from 2 to 4, RBF, and sigmoid), γ , and C . The considered hyper-parameter values are reported in Table 3. Note that in this case we could not exhaustively explore off-line the hyper-parameter space, so the optimum is unknown.

6 Software

HyperJump was implemented based on the publicly available code of BOHB (Falkner, Klein, and Hutter 2018). Moreover, we used this implementation to deploy BOHB and HB, and extend it to run ASHA. To evaluate Fabolas,

we used its publicly available implementation provided by the authors, and we also implemented a version using BO with EI and Random Search. All the optimizers were implemented in Python 3.6 and deployed on VMs equipped with 16 vCPUs and 16GB of RAM; the underlying cloud compute nodes are equipped with two AMD EPYC 7501 CPUs.

As recommended, we are making the source code of HJ, as well as the data sets used to benchmark it, available for review. Note that while the source code of HJ was submitted as a ZIP file via CMT, the data sets are too large to be submitted. We are therefore making the data sets available via a Google Drive link (Benchmarks 2021).

Note that we plan to make both HJ’s source code and the data sets used to evaluate it available for the scientific com-

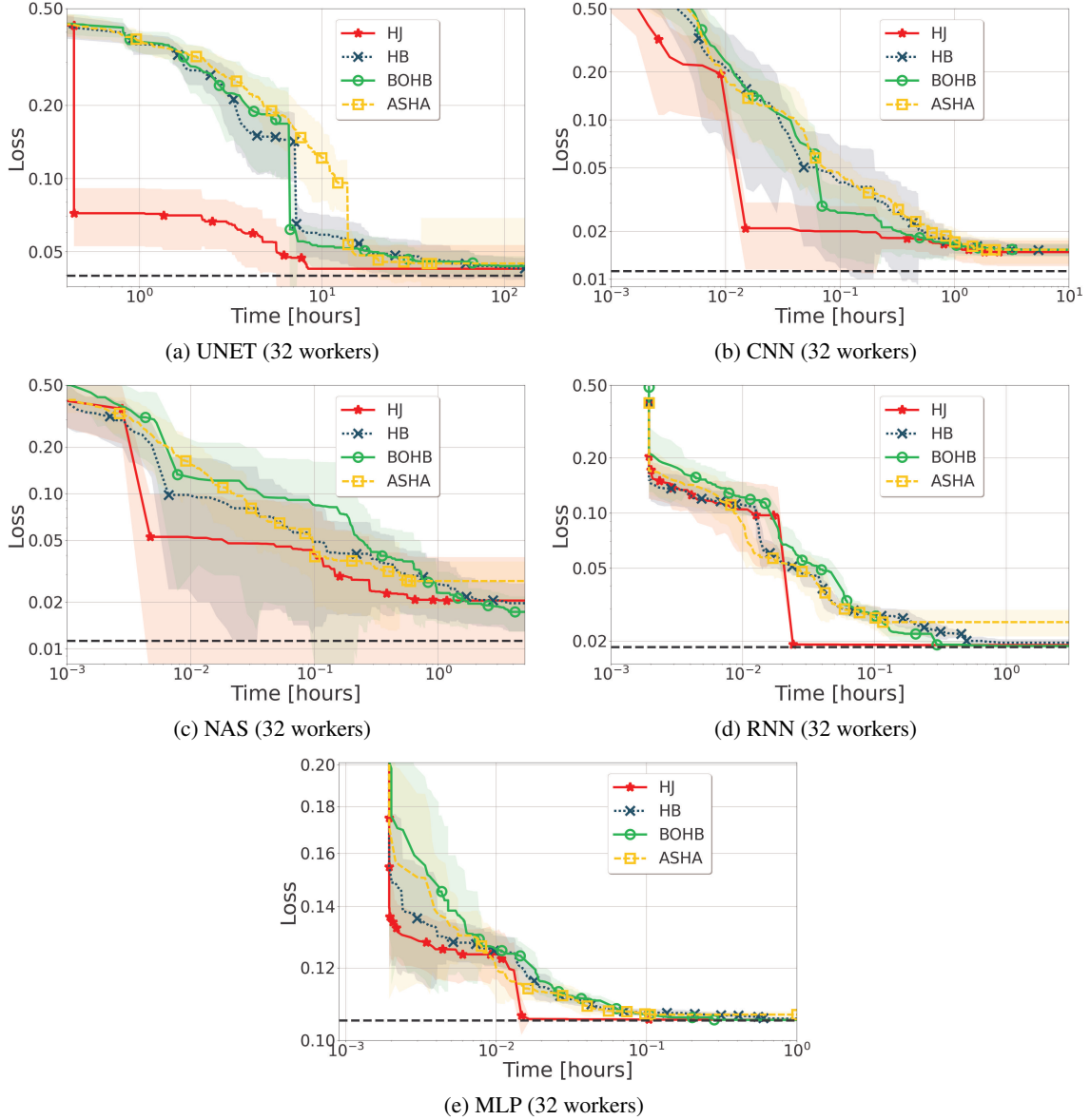


Figure 4: Comparison of HJ against other state of the art optimizers in a parallel deployment scenario using 32 workers.

munity once the paper is accepted. In order to ensure reproducibility of results, the source code already includes scripts to generate the same random seeds and reproduce the results presented in this work. We also provide instructions on how to use the scripts.

7 Additional results comparing HJ with state of the art optimizers

This section presents supplementary data regarding the comparison of HJ with respect to the set of baseline optimizers described in Section 4 of the submitted manuscript.

Figure 2 reports the average loss as a function of the wall clock time (i.e., training and recommendation time) for all the benchmarks used to evaluate HJ in a sequential deploy-

ment scenario (1 worker). Note that in this figure we are including MLP, which we had to omit from the main body of the paper due to space constraints. In order to ease visualization and comparison among benchmarks, we include in Figure 2 also the benchmarks that were already presented in Figure 1 of our submission.

Through the analysis of MLP’s data (Figure 2e), we see that in this case, analogously to the other benchmarks already discussed in the main body of the paper, HJ provides significant speed-ups to identify near optimal configurations. More in detail, HJ reduces the optimization time by approx. $10\times$ to identify close to optimum configurations compared to the most efficient baselines (HB and BOHB).

In Figure 3 and Figure 4 we report the results for the sce-

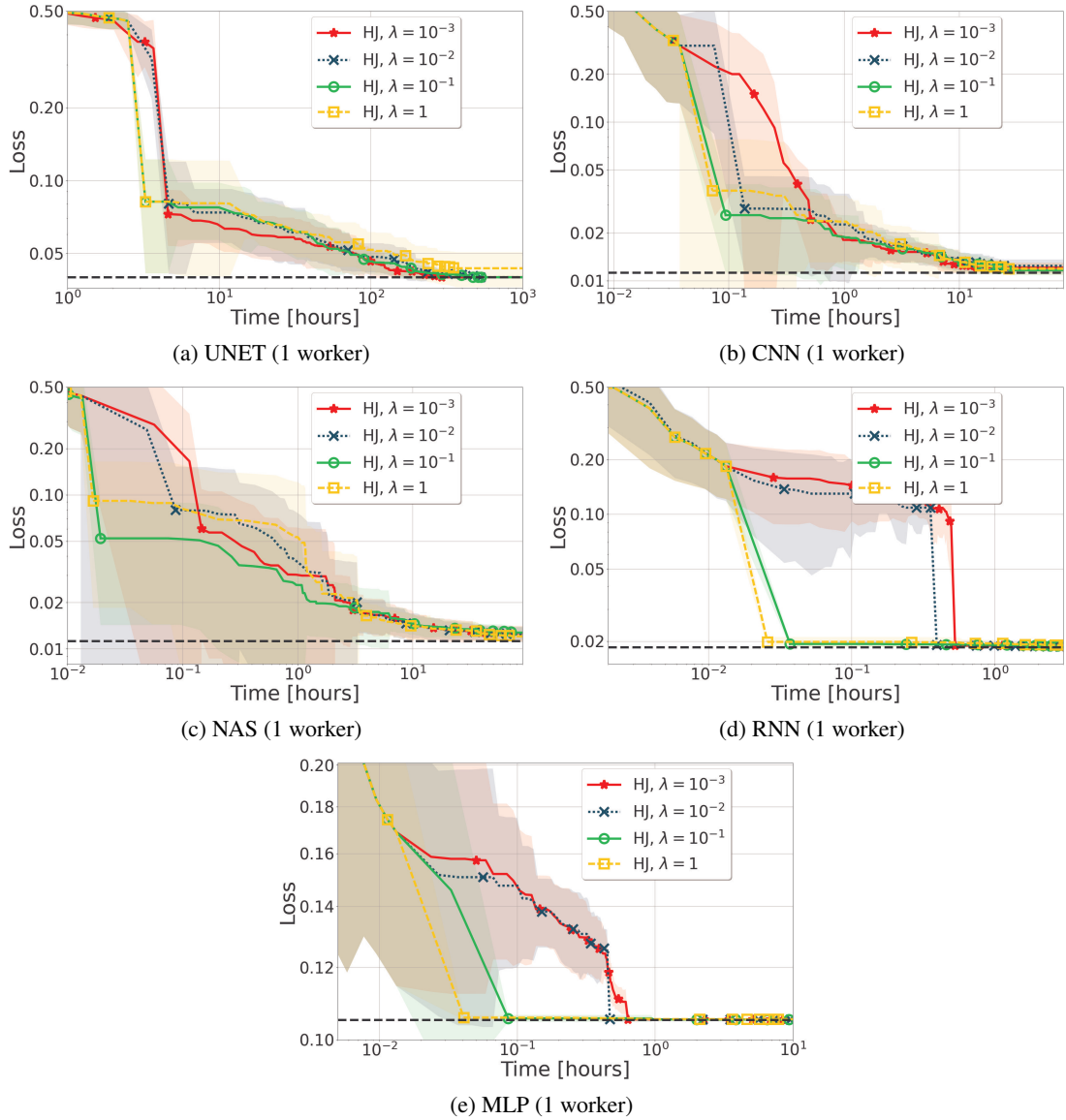


Figure 5: Performance of HyperJump when using different threshold values across several benchmarks.

nario of parallel deployments with 8 and 32 workers for all the considered benchmarks except SVM, which we could not test due to resource constraints. In this case, we report again the data for the experiments of the benchmarks already included in Figure 1 of the main body of the paper, in order to ease visualization and comparison among benchmarks.

Let us start by analyzing the data in Figure 4 for the RNN and MLP benchmarks, which were not reported in the main body of the paper in the scenario of 32 workers. When comparing the results obtained for these two benchmarks with the remaining ones, we observe a reduction in the gains that HJ achieved in the early stage of the optimization with respect to the considered baseline. A possible explanation for this is that, when using w number of parallel workers, the first w configurations tested by HJ coincide necessarily with

the first w configurations tested by HB — recall that since we assume no a priori knowledge, we cannot instantiate a model at the start of the optimization process (see Section 1) and HJ samples configurations uniformly at random, just like HB. As such, as the number of workers increases, the performance gains of HJ in the early stage of the optimization (and in particular in the first stage/bracket) tend to get closer to those of HB. Nonetheless, it is worth highlighting that also with these benchmarks, HJ achieves approximately one order of magnitude speed-ups to identify configurations that are close to optimum with respect to the best performing baselines.

Finally, the plots in Figure 3 show, as expected, trends similar to the ones already analyzed in Figure 2 and Figure 4. This is expected, considering that the scenario considered in

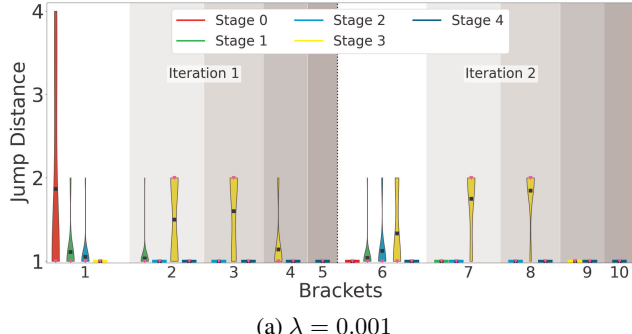
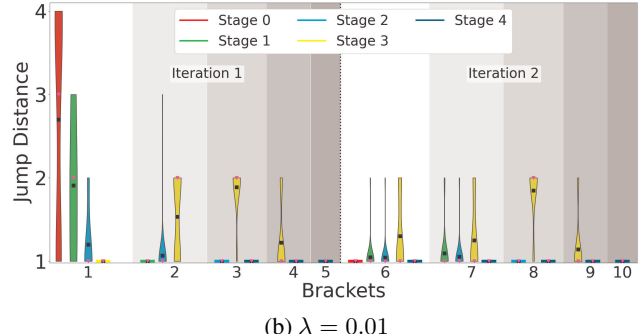
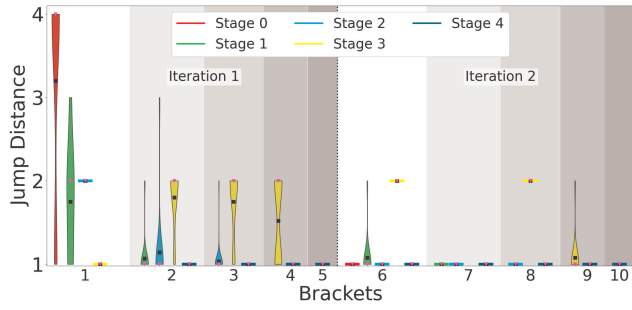
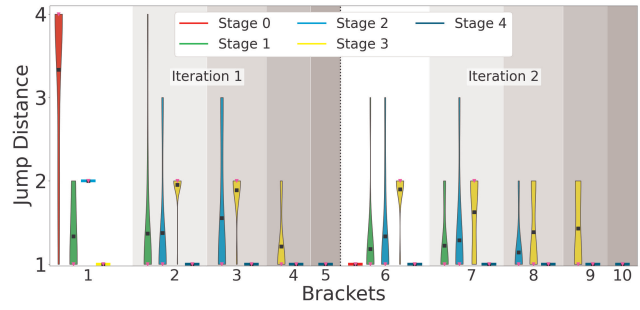
(a) $\lambda = 0.001$ (b) $\lambda = 0.01$ (c) $\lambda = 0.1$ (d) $\lambda = 1.0$

Figure 6: Evaluation of the jump length per stage for the CNN benchmark. The violin plots depict the distribution of 30 independent runs, the respective average (black square), and median (pink triangle) value.

Figure 3, i.e., 8 workers, represents a middle ground with respect to the scenarios of 1 and 32 workers, analyzed in Figure 2 and Figure 4, respectively.

8 Setting the Risk Threshold (λ)

This section reports the result of an experimental study that aimed to assess the sensitivity of HJ’s performance to the setting of the risk threshold λ . We recall that λ is the threshold that HJ uses to decide whether to consider a jump as safe and that 0.1 is its recommended setting.

To this end, we tested HJ on the same set of benchmarks (except SVM, for which we could not conduct this study due to resource constraints) using the following threshold values ($\lambda = \{10^{-3}, 10^{-2}, 10^{-1}, 1\}$) and report the corresponding results in Figure 5.

The key conclusion that can be drawn by analyzing these plots is that the performance of HJ does not vary significantly for values of λ in the $[10^{-1}, 1]$ range, with the best overall performance being achieved when using $\lambda = 10^{-1}$.

We can also observe that the use of the smallest considered threshold settings, i.e., 10^{-2} and 10^{-3} , has a negative impact on the convergence speed of HJ especially in the early stages of the optimization process. At the beginning of the optimization, in fact, models have relatively few available data. As a consequence, models have also higher uncertainty and larger threshold values need to be employed to allow HJ to shortcut HB’s search procedure. The effects are particularly noticeable with MLP and RNN, where the use of larger threshold settings (10^{-1} and 1) allows HJ to shortcut almost all of the intermediate stages of the first bracket

and to jump to the last (i.e., the full-budget) stage and identify near-optimal configurations. This phenomenon is clearly visible in Figure 6, which reports, at the granularity of each stage, the distribution, average and median of the number of stages skipped by HJ for the runs when HJ does jump, considering different threshold settings. The data in Figure 6 was produced using the CNN data-set, but analogous trends can be observed also in the other benchmarks.

By analyzing the data in Figure 6 we can also observe that in the first bracket HJ tends to perform longer jumps (i.e., skipping a larger number of stages) than in later brackets. This is due to the fact that HJ uses a risk metric (i.e., rEAR, see Section 3.2 of the main body of the paper) that is normalized by the loss of the current incumbent. As such, since in the first stage of the first bracket no incumbent is known yet (and its loss is assumed to be large, i.e., 1), the risk propensity of HJ is higher than in later brackets (when we have already identified an incumbent with loss smaller than 1).

It is however worth noting that even in the later stages of the optimization process HJ continues to avoid the testing of a significant fraction of the configurations prescribed by the HB’s logic — which is key to ensure HJ’s competitiveness throughout the optimization process. Figure 7 provides a clear experimental support for this claim by reporting the distribution, average and median of the percentage of configurations tested by HJ relative to the number of configurations tested by HB. Note that in Figure 7 we report data at the granularity of brackets in order to allow the visualization of an additional iteration of HJ and evaluate HJ’s performance

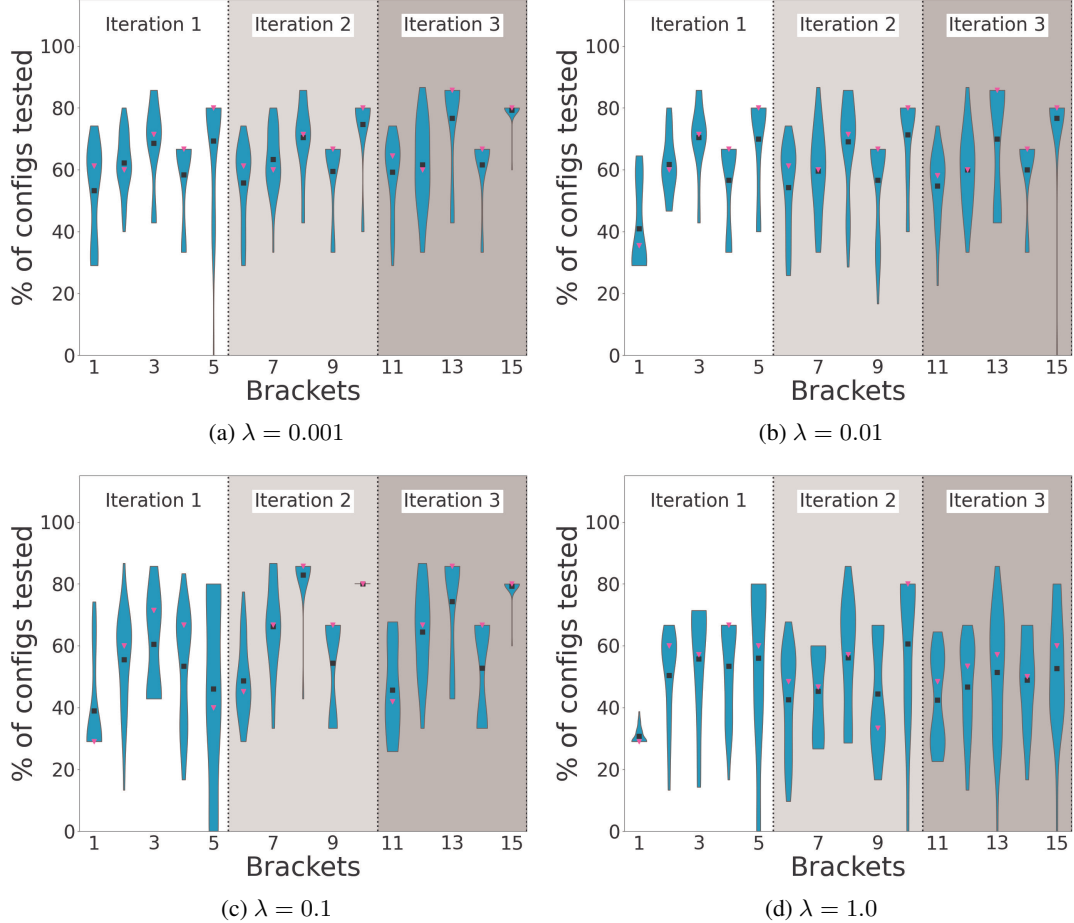


Figure 7: Evaluation of the percentage of configurations tested by HJ with respect to HB at the granularity of stage for the CNN benchmark. The violin plots depict the distribution of 30 independent runs, the respective average (black square), and median (pink triangle) value.

over a longer time scale. As expected, the largest reduction in the percentage of tested configurations is achieved in the first iteration and, in particular, in its bracket (52% and 40% on average, respectively). However, also in the later stages of the optimization process, namely in the second and third iteration, HJ still allows for skipping the testing of approximately 35% of the configurations on average when using $\lambda = 0.1$ and approximately half of the configurations in brackets, e.g., 6, 9 and 11.

Overall, in the light of this experimental data and for the benchmarks considered in this study, we can conclude that:

1. HJ provides robust performances in a relatively large range of settings for λ (i.e., $\lambda \in [10^{-1}, 1]$).
2. Setting λ below 10^{-1} tends to reduce the effectiveness of HJ by forcing it to adopt overly conservative policies.

9 Bracket Warm Starting

This section aims to evaluate the benefits stemming from using the proposed model-based methodology to warm start

a new bracket (i.e., selecting the configurations to be included in a new bracket).

To this end we report in Figure 8 the results of an experimental study, based on CNN, in which we compare the following solutions:

- HB, which selects the configuration to include in a bracket uniformly at random.
- BOHB, which uses the Tree Parzen Estimator (TPE) to approximate EI and that employs an independent model per budget. Note that we use the official implementation of BOHB and its default settings. As such, 30% of the configurations are selected uniformly at random.
- A variant of HJ where we disable the jumping mechanism and uses EI and GP as the base learner and employs an independent model per budget (similarly to BOHB). We refer to this baseline as HJ-noJ-GP-IBM in Figure 8.
- A variant similar to the previous one but instead it uses EI, GP as the base learner, and employs a single model that incorporates the budget among its features. We refer to this baseline as HJ-noJ in Figure 8.

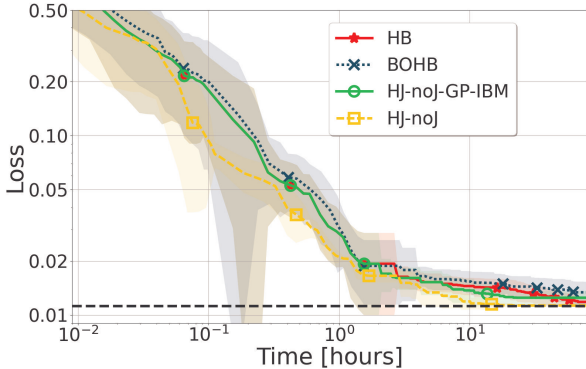


Figure 8: Comparison between different bracket warm starting techniques using CNN.

Note that, in order to focus the study solely on the evaluation of different bracket warm starting techniques, we disabled HJ’s jumping mechanism (by setting the risk threshold, λ to 0) both in the HJ-noJ and HJ-noJ-GP-IBM variants. Recall also that HJ, similarly to BOHB, samples 30% of the configurations uniformly at random to preserve the theoretical properties of HB. We preserve this behavior also in HJ-noJ and HJ-noJ-GP-IBM to ensure a fair comparison with BOHB.

By analyzing the plot we can see that the HJ-noJ approach achieves approximately 8 \times speedups to recommend the optimal configuration, as well as consistent speed-ups throughout the whole optimization process. By comparing HJ-noJ and HJ-noJ-GP-IBM we can also observe that the key factor that contributes to the HJ-noJ’s superior performance is the adoption of a single model that incorporates the budget among its features. This can be concluded by observing that the performances of HJ-noJ-GP-IBM and BOHB are very similar and recalling that the only difference between the two solutions is that the former uses EI, whereas the latter adopts TPE.

References

Benchmarks. 2021. Benchmarks used to evaluate HJ. <https://drive.google.com/drive/folders/1LaQJrMygNqTYdFZERuD08Um8t-3vp6s>.

Breiman, L. 1996. Bagging Predictors. *Machine Learning*, 24(2).

Breiman, L. 2001. Random Forests. *Machine Learning*, 45(1).

Casimiro, M.; Didona, D.; Romano, P.; Rodrigues, L.; Zwanepoel, W.; and Garlan, D. 2020. Lynceus: Cost-efficient Tuning and Provisioning of Data Analytic Jobs. In *Proceedings 20th IEEE International Conference on Distributed Computing Systems*.

Chang, C.-C.; and Lin, C.-J. 2011. LIBSVM: A Library for Support Vector Machines. *ACM Transactions on Intelligent Systems and Technology*, 2.

Deng, L. 2012. The MNIST database of handwritten digit

images for machine learning research [Best of the Web]. In *IEEE Signal Processing Magazine*, volume 29. IEEE.

Dua, D.; and Graff, C. 2017. UCI Machine Learning Repository.

Falkner, S.; Klein, A.; and Hutter, F. 2018. BOHB: Robust and Efficient Hyperparameter Optimization at Scale. In *Proceedings of the 35th International Conference on Machine Learning*, volume 80.

Klein, A.; Falkner, S.; Bartels, S.; Hennig, P.; and Hutter, F. 2017. Fast Bayesian Optimization of Machine Learning Hyperparameters on Large Datasets. In *Proceedings of the 20th International Conference on Artificial Intelligence and Statistics*, volume 54.

Klein, A.; Tiao, L. C.; Lienart, T.; Archambeau, C.; and Seeger, M. 2020. Model-based asynchronous hyperparameter and neural architecture search. *arXiv preprint arXiv:2003.10865*.

Matérn, B. 1986. *Spatial Variation*. Berlin, Germany: Springer-Verlag.

Mendes, P.; Casimiro, M.; Romano, P.; and Garlan, D. 2020. TrimTuner: Efficient Optimization of Machine Learning Jobs in the Cloud via Sub-Sampling. In *2020 28th International Symposium on Modeling, Analysis, and Simulation of Computer and Telecommunication Systems*. IEEE.

Ronneberger, O.; Fischer, P.; and Brox, T. 2015. U-Net: Convolutional Networks for Biomedical Image Segmentation. In *Medical Image Computing and Computer-Assisted Intervention – MICCAI 2015*. Springer International Publishing.

Valkov, L.; Jenatton, R.; Winkelmolen, F.; and Archambeau, C. 2018. A simple transfer-learning extension of Hyperband.

Zhang, W.; Gupta, S.; Lian, X.; and Liu, J. 2016. Staleness-Aware Async-SGD for Distributed Deep Learning. In *Proceedings of the Twenty-Fifth International Joint Conference on Artificial Intelligence, IJCAI’16*, 2350–2356. AAAI Press. ISBN 9781577357704.